
MEASURE SYNCHRONIZATION IN INTERACTING HAMILTONIAN SYSTEMS: A BRIEF REVIEW

Anupam Ghosh

Department of Complex Systems, Institute of Computer Science, Czech Academy of Sciences,
Prague 18207, Czech Republic
anupamghosh0019@gmail.com

ABSTRACT

This paper aims to review the measure synchronization, a weak form of synchronization observed in coupled Hamiltonian systems, briefly. This synchronization is characterized by a Hamiltonian system that displays either quasiperiodic or chaotic dynamics. Each system, in the presence of either linear or nonlinear coupling, shares a phase space domain with an identical invariant measure in the measure synchronized state. It is important to note that while the trajectories are identical in measure, they do not necessarily exhibit complete temporal synchrony. This synchronization has been observed in various physical systems, such as coupled pendulums, Josephson junctions, and lasers.

Keywords Measure synchronization · Hamiltonian systems · Coupled dynamical systems

1 Introduction

The word ‘synchronization’ combines two Greek words: *Syn* and *Chronos*. These words, *syn* and *chronos*, imply common (or identical) and time, respectively. Synchronization in dynamical systems refers to a phenomenon where two or more systems evolve in a coordinated manner due to the interaction or coupling between them [1, 2, 3, 4]. This phenomenon is first observed in the late seventeenth century by C. Huygens [5]. Huygens discovers that when two pendulum clocks are placed on the same wooden beam, they would eventually synchronize their oscillations, even if they have started with different initial conditions. Huygens explains this phenomenon through his theory of coupled oscillators, where the coupling force between the oscillators is transmitted through the wooden beam. Subsequent studies [1, 3] report that synchronization can occur in various forms, such as phase synchronization, frequency synchronization, and complete synchronization, depending on the nature of the dynamical systems and the coupling between them. The study of synchronization in dynamical systems is of great interest in many fields, including physics, biology, neuroscience, and engineering, and has important applications in information processing, communication, and control [6, 2, 3].

Synchronization is observed in various dynamical systems, including coupled dissipative and Hamiltonian systems. A Hamiltonian system [7] is a conservative system that conserves the phase space volume with time following Liouville’s theorem. The motion of the system is described by a set of differential equations, known as Hamilton’s equations, that describe how the generalized coordinates and corresponding generalized momentum variables of the system evolve over time. The synchronization in Hamiltonian systems results from the exchange and conservation of energy between the interconnected components. This can be observed in systems like coupled pendulums or celestial bodies, where the shared energy leads to synchronized motion without any net loss. A dissipative system [8], on the other hand, is a system that loses energy over time due to internal friction, viscosity, or other forms of energy dissipation. A set of differential equations also describes the motion of any dissipative system, but the equations include terms that represent the dissipation of energy. As a result, the phase space volume collapses with evolution time, and the system eventually reaches an attractor or a steady state. Overall, the dynamics of coupled dissipative and coupled Hamiltonian systems differ, and this dissimilarity leads to different types of synchronization in both categories. However, we restrict ourselves to study measure synchronization [9], observed in coupled Hamiltonian systems, in this review.

The synchronization phenomenon in Hamiltonian systems has been observed in various physical systems, including coupled pendulums, Josephson junctions, and lasers [10, 11, 12, 13]. The understanding of synchronization in such systems has led to the development of several analytical and numerical techniques and has found applications in various fields. Therefore, studying synchronization in coupled Hamiltonian systems is a complex and fascinating topic that has attracted significant research interest. Measure synchronization (MS) [9] is a phenomenon observed in coupled Hamiltonian systems where the distributions of the measures of two or more systems become synchronized, while the individual trajectories of each system may still vary widely. Here, the word ‘measure’ refers to the Lebesgue measure [14], a mathematical concept used to measure the size or volume of subsets of Euclidean space. The onset of MS implies that the statistical properties of the states of the systems are highly similar, but the specific values of their coordinates may differ significantly.

MS is observed in a coupled-pendulum system with a common beam serving as the coupling medium, resulting in indirect coupling between the pendulums [15]. This study [15] focuses on the role of the common beam in the emergence of MS and aims to contribute to the conventional understanding of synchronization (proposed by C. Huygens [5]) by emphasizing the crucial role played by the common beam. The coupled-pendulum system suspended from the common beam can reach MS by adjusting the mass ratio of the common beam to that of each pendulum. Classical manifestations of MS have also been observed across various model systems, including the ϕ^4 model [16], Duffing model [17], and coupled bosonic Josephson junction [10]. The classical concept of MS has further been extended into quantum mechanics, and it has been demonstrated that quantum MS emerges in coupled quantum many-body systems [11]. In the quantum domain, MS is characterized by purely quantum mechanical phenomena; specifically, collapses and revivals dynamics become synchronized once the system reaches a state of quantum MS. Thus, MS is observed in a wide range of physical systems, such as coupled oscillators, coupled maps, and coupled particles. To this end, the partial MS [18] manifests in systems comprising more than two suitably interconnected subsystems. This phenomenon is notably evident in systems involving three subsystems, wherein a distinct pattern emerges: the first subsystem may exhibit synchronization with the third subsystem while remaining uncoordinated with the second subsystem. This intriguing phenomenon is termed partial MS [17, 19].

The structure of this paper is organized as follows: firstly, we explore an analytical understanding of the fundamental mechanism underlying MS in Sec. 2. Subsequently, we inspect two broad categories of MS transitions in Sec. 3. In this section, we also discuss various indices found in the existing literature, which facilitate the quantitative detection of MS within dynamical systems. Furthermore, we emphasize the significance of the initial condition selection in this context. Sec. 4 is dedicated to discussions surrounding partial MS. Sec. 5 delves into the framework of occasional coupling as a tool for studying MS. Sec. 6 investigates the exploration of MS within quantum Hamiltonian systems. Finally, in Sec. 7, we summarize MS and discuss different possible future aspects of MS in interacting dynamical systems.

2 Mechanism of MS

In this section, we analytically understand the underlying mechanism of MS, as reported by Hampton and Zanette [9]. In this regard, we adopt the following example of coupled Hamiltonian systems [9]:

$$H = \frac{\omega_1^2}{2} + \frac{\omega_2^2}{2} - \frac{K}{2} \cos(\theta_2 - \theta_1). \quad (1)$$

Here, two dynamical systems with Hamiltonian $H_i = \frac{\omega_i^2}{2}$, $i = 1, 2$, are interacting with each other through the term $\frac{K}{2} \cos(\theta_2 - \theta_1)$. The strength of this interaction is measured by the parameter K . The equations of motion in canonical form can be expressed as:

$$\dot{\theta}_1 = \omega_1, \quad (2a)$$

$$\dot{\theta}_2 = \omega_2, \quad (2b)$$

$$\dot{\omega}_1 = \frac{K}{2} \sin(\theta_2 - \theta_1), \quad (2c)$$

$$\dot{\omega}_2 = \frac{K}{2} \sin(\theta_1 - \theta_2). \quad (2d)$$

We begin with $K = 0$, i.e., when no interaction is activated between the Hamiltonian systems. In this case, the angle variable θ_i changes with a constant rate ω_i , which further help us to write:

$$\omega_1(t) + \omega_2(t) = \omega_1(0) + \omega_2(0) = \Omega, \quad (3)$$

where Ω is a constant. The angle variables can also be written as:

$$\theta_1(t) + \theta_2(t) = \theta_1(0) + \theta_2(0) + \Omega t. \quad (4)$$

Now, introduce two new variables $\xi(t)$ and $\nu(t)$ as follows:

$$\xi(t) = \theta_1(t) - \theta_2(t), \quad (5a)$$

$$\omega_{1,2}(t) = \omega_{1,2}(0) \pm \nu(t). \quad (5b)$$

In terms of the newly defined variables, we can write:

$$\dot{\xi}(t) = \omega_0 + 2\nu, \quad (6a)$$

$$\dot{\nu}(t) = -\frac{K}{2} \sin \xi, \quad (6b)$$

where $\omega_0 = \omega_1(0) - \omega_2(0)$. Differentiating Eq. 6a and with the help of Eq. 6b, we can write:

$$\ddot{\xi}(t) + K \sin \xi = 0. \quad (7)$$

Thus, Eq. 7 represents a pendulum with total energy:

$$E = \frac{\dot{\xi}^2(t)}{2} - K \cos \xi(t), \quad (8a)$$

$$= \frac{\dot{\xi}^2(0)}{2} - K \cos \xi(0). \quad (8b)$$

The total energy E remains invariant with the evolution time t . When $E > K$, $\xi(t)$ changes monotonically with time t , and $|\dot{\xi}|$ oscillates between $\sqrt{2(E-K)}$ and $\sqrt{2(E+K)}$. This kind of dynamics is termed ‘rotation’. In contrast, an oscillation of the pendulum is detected around the fixed point $\xi = 0$ for $E < K$. The variables ξ and $\dot{\xi}$ evolve symmetrically around $\xi = 0$. These two different types of dynamics, rotations and oscillations, are separated by the separatrix $E = K$. The threshold value of the coupling strength K^c is given by:

$$K^c = \frac{\dot{\xi}^2(0)}{2(1 + \cos \xi(0))}, \quad (9)$$

with the total energy $E = K^c + (K^c - K) \cos \xi(0)$.

The original frequency variables become $\omega_{1,2} = (\Omega \pm \dot{\xi})/2$. For a significantly smaller value of K , $\dot{\xi}$ exhibits small oscillation around $\sqrt{E} \simeq \sqrt{2K^c}$, and frequencies ω_1 and ω_2 oscillate around two separated values $\Omega/2 + \sqrt{K^c}/2$ and $\Omega/2 - \sqrt{K^c}/2$, respectively. A further increase in K , as long as $K < K^c$, the frequencies evolve within two non-overlapping intervals $[\Omega/2 + \sqrt{(E-K)}/2, \Omega/2 + \sqrt{(E+K)}/2]$ and $[\Omega/2 - \sqrt{(E-K)}/2, \Omega/2 - \sqrt{(E+K)}/2]$. It is noteworthy that as the coupling strength K approaches its threshold value, both the lower boundary of the upper interval and the upper boundary of the lower interval converge toward the value of $\Omega/2$. Finally, as soon as K crosses K^c , $\dot{\xi}$ exhibits oscillation around zero with an amplitude of $\sqrt{2(E+K)}$, and both frequencies $\omega_{1,2}$ vary within the interval $[\Omega/2 + \sqrt{(E+K)}/2, \Omega/2 - \sqrt{(E+K)}/2]$, i.e., two separated frequency intervals merge and become a single interval as K crosses K^c . In other words, both frequencies share a phase space domain with an identical invariant measure when K crosses K^c .

This analytical analysis of MS has also been studied numerically by employing the Poincaré section analysis [20]. These Poincaré sections are constructed in the projected phase planes (θ_1, ω_1) and (θ_2, ω_2) , respectively. This investigation provides convincing evidence supporting the assertion that the occurrence of MS is intrinsically associated with the phenomenon of separatrix crossing, which serves as the overarching mechanism underlying MS.

3 Types of MS transition

The term ‘MS transition’ denotes the transition from a desynchronized state to a MS state, which occurs at a critical value of the coupling parameter. The synchronized state can manifest as either a quasiperiodic or chaotic solution of the full coupled system. It is useful to categorize the transitions from the desynchronized state to the corresponding synchronized state in this paper as (i) quasiperiodic to quasiperiodic MS and (ii) quasiperiodic to chaotic MS.

3.1 MS transition: quasiperiodic to quasiperiodic dynamics

Let us consider a bidirectionally coupled Hamiltonian systems (the ϕ^4 -system [16], to be specific), which can be characterized by the following Hamiltonian:

$$\begin{aligned} H &= \frac{p_1^2}{2} + \frac{q_1^4}{4} + \frac{p_2^2}{2} + \frac{q_2^4}{4} + K_Q (q_1 - q_2)^2, \\ &= H_1(q_1, p_1) + H_2(q_2, p_2) + H_c. \end{aligned} \quad (10)$$

The system under consideration involves a real non-negative parameter, denoted by K_Q , which represents the coupling strength between two one degree-of-freedom subsystems described by $H_i(q_i, p_i)$. The coupling is provided by H_c . The corresponding equations of motion in canonical form can be expressed as follows:

$$\dot{q}_1 = p_1, \quad (11a)$$

$$\dot{q}_2 = p_2, \quad (11b)$$

$$\dot{p}_1 = -q_1^3 + 2K_Q (q_2 - q_1), \quad (11c)$$

$$\dot{p}_2 = -q_2^3 + 2K_Q (q_1 - q_2). \quad (11d)$$

Upon reaching the MS state, the long-term average of any variable across distinct sites becomes equal. Hence, utilizing averages of specific physical quantities to represent the transition to MS state between various oscillators becomes beneficial. A suitable candidate for such averages is the long-term average of the bare energies of the interacting oscillators:

$$E_i = \frac{1}{T_f} \int_0^{T_f} H_i(q_i, p_i) dt, \quad (12)$$

where T_f represents the final time up to which the system has evolved. In a synchronized state, the difference in average bare energies ($\Delta E := E_1 - E_2$) should be nearly zero. A desynchronized state between the interacting oscillators can be inferred from a non-zero value of ΔE when plotted against the coupling strength parameter.

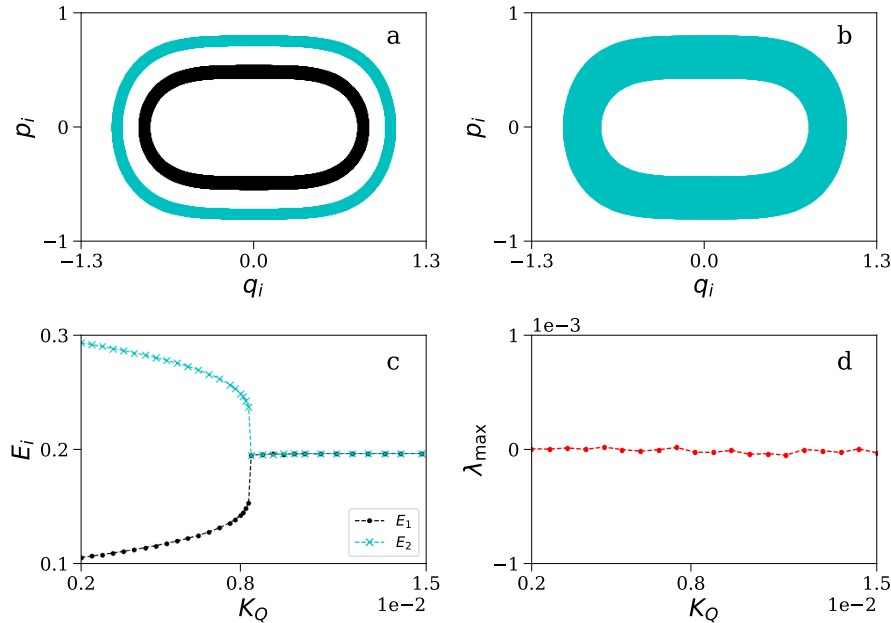


Figure 1: The black and cyan colours in subplots (a)–(c) correspond to the first and second oscillators. (a) Desynchronized state at $K_Q = 0.6 \times 10^{-2}$. (b) Synchronized state at $K_Q = 1 \times 10^{-2}$. (c) Average bare energies (E_i) are calculated, using Eq. 12, as a function of K_Q . (d) The maximum Lyapunov exponent (λ_{\max}) is plotted as a function of K_Q . In both cases, desynchronized and synchronized, the four-dimensional oscillator (Eq. 11) exhibits quasiperiodic oscillations.

The phase space dynamics of a Hamiltonian system is profoundly influenced by the structure of the phase space and the initial conditions, as is the case with MS, a noteworthy phenomenon. This dependence on initial conditions arises

from two primary factors: Firstly, Hamiltonian systems lack attractors, resulting in each orbit displaying distinct asymptotic dynamical behaviour compared to others. Secondly, an initial condition uniquely determines the energy of the autonomous Hamiltonian system, effectively treating the initial condition as a system parameter, a departure from dissipative systems. Consequently, altering the initial conditions inevitably leads to divergent system dynamics; even a slight adjustment may shift dynamics from quasiperiodic to chaotic or vice versa. However, we start investigating the MS transition with initial condition $(q_1(0), q_2(0), p_1(0), p_2(0)) = (0.0, 0.0, \sqrt{0.2}, \sqrt{0.6})$ and $H = 0.4$ [18]. After calculating E_i at different values of K_Q , we have obtained a transition to MS state while K_Q is varying within the range $[0.2 \times 10^{-2}, 1.5 \times 10^{-2}]$. Figures 1a and 1b depict the projected phase space trajectories in the two-dimensional phase space at $K_Q = 0.6 \times 10^{-2}$ and 1×10^{-2} , respectively. Figure 1a illustrates a desynchronized state showing that the two subsystems occupy distinct regions of the projected two-dimensional phase space. In contrast, we observe the synchronized state at $K_Q = 1 \times 10^{-2}$ (Fig. 1b). The average bare energies E_i are plotted as a function of K_Q in Fig. 1c. At lower values of K_Q , E_i are non-overlapping; for $K_Q \geq K_Q^c$ (where $K_Q^c \simeq 0.84 \times 10^{-2}$), E_i overlapped, implying the occurrence of MS state in this range of K_Q .

Finally, we have calculated the maximum Lyapunov exponent (λ_{\max}) as a function of coupling strength K_Q and plotted in Fig. 1d. The maximum Lyapunov exponent [8] measures the rate of divergence or convergence of nearby trajectories in phase space. It quantifies the sensitivity of the system's behaviour to small changes in the initial conditions. A positive λ_{\max} indicates that nearby trajectories in phase space diverge exponentially fast, implying chaotic behaviour. In contrast, a zero λ_{\max} indicates a quasiperiodic motion. Therefore, Fig. 1d supports to conclude that Eq. 11 exhibits quasiperiodic motion for $K_Q \in [0.2 \times 10^{-2}, 1.5 \times 10^{-2}]$. It is worth noting that the subscript 'Q' in K_Q is used to indicate a quasiperiodic system trajectory that is present both before and after the synchronization transition.

3.1.1 Phase-based order parameters of MS

Hampton and Zanette [9] have introduced two order parameters, denoted as η and f , which serve as tools for discerning the MS transition based on the phase dynamics of the interacting oscillators. Let $\phi_1(t)$ and $\phi_2(t)$ be the instantaneous phases of the respective oscillators calculated using the standard Hilbert transform [1] of phase space variables. In the desynchronized state, the phase difference ($\Delta\phi := \phi_1 - \phi_2$) changes, on average, linearly with evolution time, i.e., $\Delta\phi(t) \approx \eta t + \Delta\phi(0)$. This observation arises due to the difference in main frequencies between the orbits. This order parameter, η , can be defined as:

$$\eta = \left| \lim_{t \rightarrow \infty} \frac{\Delta\phi(t)}{t} \right|. \quad (13)$$

On the contrary, when the two orbits achieve synchronization and share a common domain in phase space, $\Delta\phi(t)$ undergoes oscillations with a characteristic frequency f around a steady value, i.e.,

$$\Delta\phi(t) = \Delta\phi(t + 2\pi/f), \quad (14)$$

where f is the most dominant Fourier component of $\Delta\phi(t)$. In the synchronized region, η reaches to a value of 0, while f remains finite. Conversely, in the desynchronized region, the opposite scenario emerges. The pronounced changes in the values of η and f at this transition point signify its critical nature. However, neither η nor f adheres to any power law scaling in the vicinity of the critical point [9, 21, 22].

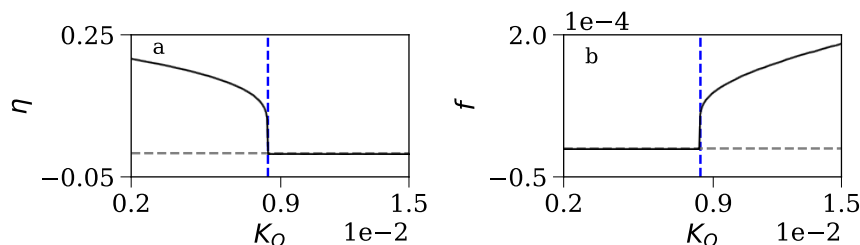


Figure 2: (a) The first phase-based index η is plotted as a function of K_Q . (b) The second index, f , is plotted as a function of K_Q . In both subplots, the vertical blue dashed lines correspond to $K_Q = K_Q^c$. The horizontal gray dashed lines correspond to zero magnitudes of these indices.

These phase-based indices are plotted as a function of K_Q in Fig. 2. The first index η , in Fig. 2a, has non-zero values initially; on reaching the critical point $K_Q = K_Q^c$, η reaches zero and remains zero in the synchronized region ($K_Q > K_Q^c$). The reverse scenario is observed for the second index f , as depicted in Fig. 2b.

3.1.2 Critical behaviour of MS

A critical behaviour of MS has also been examined after calculating another energy-based index, the average interaction energy between the interacting oscillators as function of coupling strength. Along with ΔE , the aforesaid average interaction energy has also been used in the literature to study the transition to MS [16]. We can, therefore, define the average interaction energy (E_{int}) between $H_1(q_1, p_1)$ and $H_2(q_2, p_2)$ as follows:

$$E_{\text{int}} = \frac{1}{T_f} \left| \int_0^{T_f} H_c dt \right|, \quad (15)$$

where $H_c = K_Q(q_1 - q_2)^2$ for the coupled ϕ^4 -systems (Eq. 10). We have plotted the calculated E_{int} as a function of K_Q in Fig. 3a. Initially, E_{int} increases monotonically with the increase in K_Q up to $K_Q = K_Q^c$ and decreases thereafter. In other words, a kink is visible at $K_Q = K_Q^c$. For further confirmation, the first-order derivative of E_{int} with respect to K_Q has been plotted as a function of K_Q (Fig. 3b). The discontinuity at $K_Q = K_Q^c$ in Fig. 3b mathematically supports the existence of this kink.

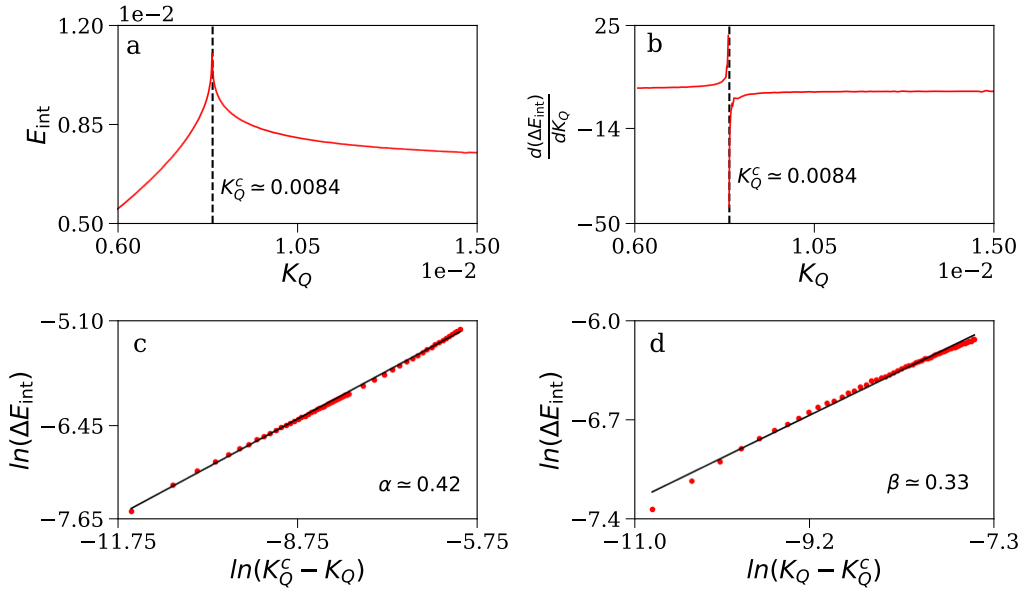


Figure 3: (a) The average interaction energy E_{int} has been plotted as a function of K_Q . (b) The first-order derivative, $\frac{d(\Delta E_{\text{int}})}{dK_Q}$, is plotted at different values of K_Q . Both subplots support the existence of a critical point at $K_Q = K_Q^c$. (c) The critical exponent α has been calculated while Eq. 11 reaches the critical point. (d) The critical exponent β has been calculated after the occurrence of the MS transition.

In order to study the critical behaviour associated with this MS transition, we can define the difference in interaction energy as $\Delta E_{\text{int}} := (E_{\text{int}}^c - E_{\text{int}})$, where E_{int}^c is the average interaction energy at $K_Q = K_Q^c$. This ΔE_{int} follows some power laws on either side of critical point $K_Q = K_Q^c$, as mentioned follows:

$$\Delta E_{\text{int}} \propto \begin{cases} (K_Q^c - K_Q)^\alpha & \text{for } K_Q < K_Q^c, \\ (K_Q - K_Q^c)^\beta & \text{for } K_Q > K_Q^c, \end{cases} \quad (16)$$

where α and β are the critical exponents. For the example in hand, the calculated critical exponents are $\alpha = 0.42$ and $\beta = 0.33$ (Figs. 3c and 3d).

Wang et al. [16] extensively analyze the scaling law behind MS in coupled ϕ^4 systems (with a different set of initial conditions) by computing the average interaction energy. They numerically verify different scaling laws before and after MS state, with critical exponents of $1/3$ and $1/2$. We can also detect this critical behaviour of MS in a two-species bosonic Josephson junction [10] and coupled-pendulum system hung from a common beam [15]. In both cases, the power law scaling near the MS transition is associated with a critical exponent of $1/2$. Gupta et al. [22] report the values of these power law indices as 0.83 and 1.30 respectively. In passing, Hampton and Zanette [9] have also investigated this critical logarithmic singularity; However, due to their use of an averaged quantity as the order parameter for the calculation, they do not identify the scaling law or the critical exponent.

3.2 MS transition: quasiperiodic to chaotic dynamics

Here, we have adopted another Hamiltonian system, as reported by Ghosh et al. [23], to characterize a system exhibiting a quasiperiodic trajectory prior to the MS transition, which subsequently becomes chaotic. The explicit form of Hamiltonian is as follows:

$$\begin{aligned} H &= \frac{I_1^2}{2} + \frac{I_2^2}{2} - \frac{K_C}{2} [\cos(\theta_1 - 3\theta_2) + \cos(3\theta_1 - \theta_2)], \\ &= H_1(I_1) + H_2(I_2) + H_C. \end{aligned} \quad (17)$$

The function H_C used in Eq. 17 differs from the one used in the preceding Hamiltonian (Eq. 10). The coupling strength parameter, K_C , is a non-negative real number. The corresponding canonical equations of motion are given by:

$$\dot{\theta}_1 = I_1, \quad (18a)$$

$$\dot{\theta}_2 = I_2, \quad (18b)$$

$$\dot{I}_1 = -\frac{K_C}{2} [\sin(\theta_1 - 3\theta_2) + 3\sin(3\theta_1 - \theta_2)], \quad (18c)$$

$$\dot{I}_2 = \frac{K_C}{2} [3\sin(\theta_1 - 3\theta_2) + \sin(3\theta_1 - \theta_2)]. \quad (18d)$$

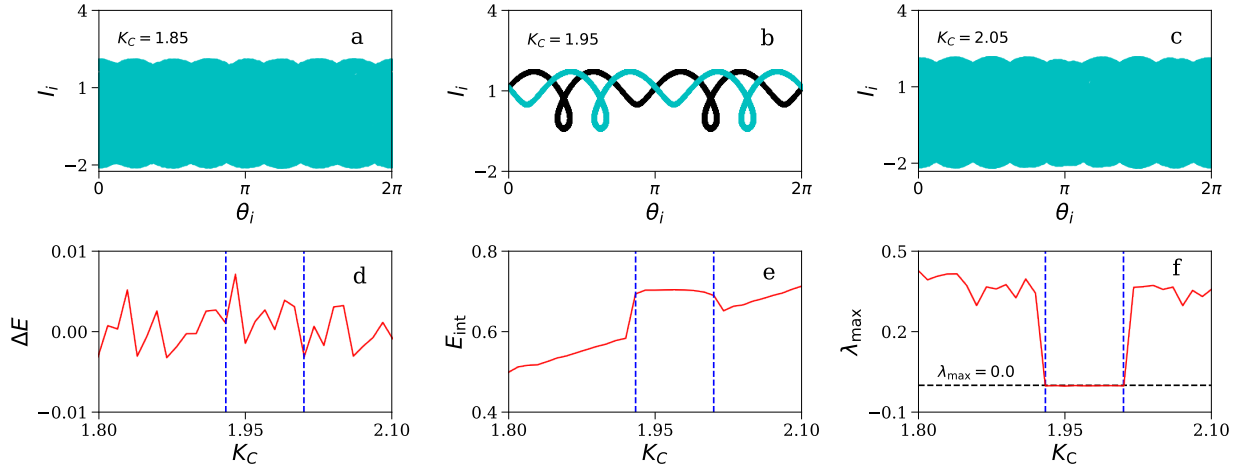


Figure 4: Synchronized state is observed in subplots (a) and (c) correspond to $K_C = 1.85$ and 2.05 . Subplot (b) depicts the desynchronized state at $K_C = 1.95$. The black and cyan colours in both plots correspond to the first and second oscillators. (d) The difference in average bare energies (ΔE) is plotted as function of K_C . (e) The average interaction energy (E_{int}) is plotted as a function of K_C . (f) The maximum Lyapunov exponent (λ_{max}) is plotted at different values of K_C . The regions within the vertical blue dashed lines in subplots (d), (e) and (f) represent the desynchronization window.

The subscript ‘C’ in K_C indicates that the four-dimensional oscillator (Eq. 18) displays chaotic dynamics upon transitioning to the synchronized state. However, similar to the previous example, quasiperiodic dynamics exist in the desynchronized state. When the initial condition is $(\theta_1(0), \theta_2(0), I_1(0), I_2(0)) = (4.39679, \pi/2, 0.975717, 1.58675)$ with $H = 0.2$, a ‘desynchronization window’ is observed for values of K_C between 1.93 and 2.01 [23]. At $K_C = 1.95$, a value within the aforesaid window, the desynchronized state is confirmed by the non-overlapping phase space plots shown in Fig. 4b for the two subsystems. Conversely, Figs. 4a and 4c depict synchronized state at $K_C = 1.85$ and 2.05 , respectively. Unlike the previous example, the first index ΔE fails to detect the desynchronization window (Fig. 4d), while the other index E_{int} effectively identifies it (Fig. 4e). The persistence of long-term chaotic transients contributes to the emergence of non-zero values of ΔE in the synchronized state [22]. The convergence of ΔE towards zero necessitates the evolution of the system for a substantially extended period (i.e., T_f must be very large).

Finally, we have calculated the maximum Lyapunov exponent (λ_{max}) as a function of K_C and plotted it in Fig. 4f. It (λ_{max}) has non-zero values outside the desynchronization window and has zero values for $K_C \in [1.93, 2.01]$. Hence, a direct association exists between the MS transition and the transition from quasiperiodicity to chaotic dynamics, and

λ_{\max} can be used as a control parameter to study this kind of MS transition [16, 24]. In other words, if the coupled Hamiltonian system exhibits chaotic dynamics, the interacting oscillators are in MS state. A key feature of chaotic dynamics is their recurrence property, which implies that a chaotic system revisits a specific region of its phase space repeatedly, with arbitrarily small distances between these visits. This key feature is responsible for the aforementioned direct connection.

Note that the indices η (Eq. 13) and f (Eq. 14) are not considered as recommended order parameters to study MS transition from quasiperiodic to chaotic dynamics. While η can identify quasiperiodic desynchronized regions, it can not identify the MS transition from quasiperiodicity to chaos. This limitation originates from the fact that oscillators are not precisely phase-locked in the chaotic region, and the phase difference ($\Delta\phi$) exhibits arbitrary jumps of $n\pi$ radians between synchronous segments. Furthermore, within the chaotic regime, there might not exist a dominant Fourier component, referred to as f , of the dynamical variable $\Delta\phi$. Consequently, the Fourier component f becomes nonexistent in the synchronized region. Besides, the critical transition, as discussed in Sec. 3.1.2, does not visible in this category of MS transition [16].

3.3 Choice of initial condition

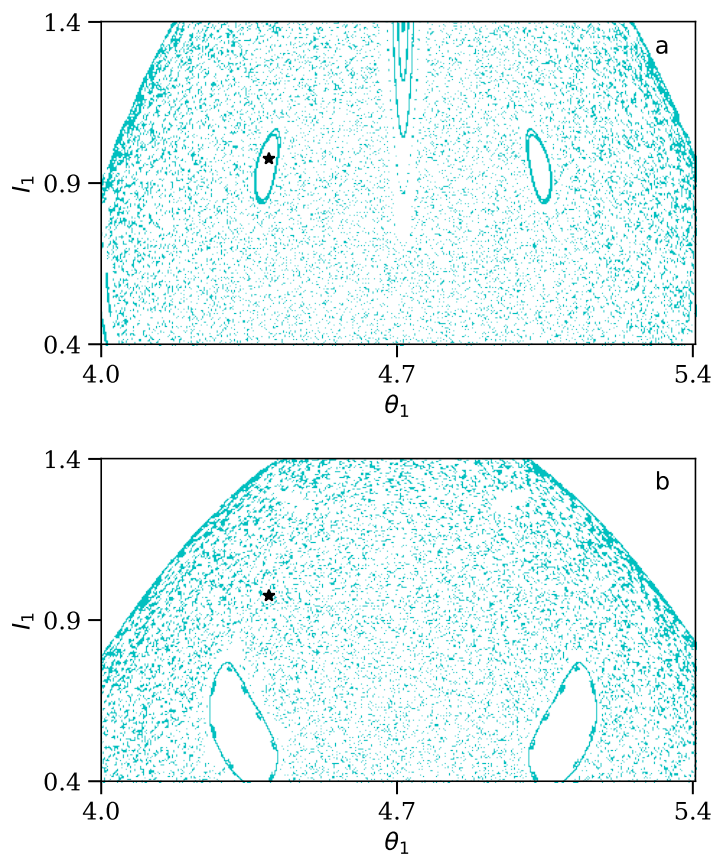


Figure 5: The Poincaré sections of the first subsystem are presented in subplots (a) and (b), utilizing fifty distinct sets of initial conditions. Subplot (a) corresponds to $K_C = 1.95$, while subplot (b) is associated with $K_C = 0.975$. Notably, the black stars in both subplots represent the initial condition, $(\theta_1(0), I_1(0)) = (4.39679, 0.975717)$, used in Sec. 3.2. A desynchronized state is observed if an initial condition lies within the resonance islands; conversely, if it falls outside these regions, an MS state manifests.

The selection of an initial condition plays an important role in a Hamiltonian system [7]. Consequently, each orbit has the potential to exhibit asymptotically distinct dynamical behaviours in comparison to any other orbits. In a Hamiltonian system, an initial condition prescribes the total energy of the autonomous system. This implies that the initial condition effectively plays the role of a system parameter, in contrast to the behaviour observed in dissipative

systems [8]. Hence, it becomes apparent that even a slight alteration in the choice of initial conditions can induce a considerable transformation in the system's behaviour. A mere modification in the initial condition can instigate a shift in dynamics, potentially transitioning from chaotic to quasiperiodic behaviour or vice versa.

Here, we adopt the Poincaré section analysis [20] to study the effect of choosing an appropriate initial condition in Hamiltonian systems. In order to employ the Poincaré section analysis, we evolve Eq. 18 for a fixed value of K_C and collect $(\theta_1(t), I_1(t))$ values when $\theta_2(t) = \pi/2$ and $I_2(t) > 0$. Finally, we repeat this process for different sets of initial conditions with the constraint that the total Hamiltonian value remains unaltered (i.e., $H = 0.2$ in Eq. 17). Figure 5 depicts the existence of a few resonance islands in the chaotic sea for two different values of K_C . As depicted in Fig. 5a, the system characterized by a constant value of coupling strength $K_C = 1.95$, there exists a collection of initial conditions situated within the resonance islands yield quasiperiodic motion. The specific initial condition — $(\theta_1(0), I_1(0)) = (4.39679, 0.975717)$, which eventually emerges the desynchronized state — adopted in Sec. 3.2 lies within one such resonance island, as shown using the black star marker in Fig. 5a. In the other subplot, Fig. 5b, the location of the aforesaid adopted initial condition is no longer within those islands but in the chaotic sea. Consequently, a change in dynamics is detected, which further yields the occurrence of an MS state. Note that the identification of chaotic dynamics is challenging when the initial conditions are close to the outer boundaries of these islands. In such cases, a trajectory that initially displays regular behaviour over an extended time interval and eventually reveals its intrinsic chaotic nature after a long transient. The corresponding trajectory is generally termed 'sticky orbit' [25]. In the case of sticky orbits, one must evolve the system for an immense amount of time to confirm the MS state.

The conclusion of Fig. 5 remains invariant even though we analyze the Poincaré sections in the (θ_2, I_2) plane. Similar resonance islands are also detected while we extend our study to the MS transition of the first category (Sec. 3.1). Any initial condition outside of these islands leads to the occurrence of an MS state [23].

3.4 Other indices to detect MS

MS in a two coupled bosonic Josephson junction model has been studied using the Poincaré section analysis [10] and reported that the separatrix crossing is responsible to reaching the MS state. In addition to these techniques, one can always return to the first principle of MS and compare the joint probability density functions of the coupled systems to verify whether the systems share unaltered measures quantitatively [23].

Another article [26] demonstrates the presence of MS in a Hamiltonian system associated with the nonlinear Schrödinger equation. Furthermore, it discusses the transition from quasiperiodic measure desynchronization to quasiperiodic MS and from quasiperiodic measure desynchronization to chaotic MS are generic characteristics that define the relationship among coupled nonlinear Schrödinger equation subsystems. A recent paper [27] investigates MS in a two-population network of coupled metronome systems. The system comprises multiple identical metronomes on two swing boards connected by a spring. Each swing board represents a single population. The primary objective is to examine the collective dynamics of the multi-population Hamiltonian induced by the coupling strength, which includes inter-population and intra-population couplings. MS and partial MS are observed—the occurrence of these MS states is studied by analyzing the Poincaré sections of the Hamiltonian system.

The study of MS has additionally been carried out within a framework comprising of two nonlinearly coupled oscillators [22, 19]. In these studies, different types of dynamical states, such as quasiperiodic, chaotic, MS, and desynchronized, along with their respective transitions from one to another, have been observed and quantified by varying the coupling parameter.

Until now, our discussions have revolved around MS in Hamiltonian systems constituted of two interacting subsystems. In Sec. 4, we explore MS in the Hamiltonian systems composed of more than two interacting subsystems. Analogous to the three-body problem in classical mechanics, the coupled three-oscillator system unveils a richer and more intricate dynamic landscape compared to its two-oscillator counterpart. This intricate behaviour introduces novel states and transition phenomena. This entails extending prior notions and research about MS while retaining the essential insights they offer.

4 Partial MS

MS has been a focal point of inquiry in many-body quantum systems, particularly within the domain of quantum spin chains. In quantum communication theory, these quantum spin chains are envisioned as potential 'quantum wires' capable of connecting quantum devices. In the literature, significant research efforts have been directed toward examining spin chains as convincing quantum channels necessary for quantum state transfer and entanglement dynamics [28, 29, 30]. When two quantum spin chains are coupled, they initiate the redistribution of quantum correlations within each chain and establish correlations between themselves as time evolves. The quantum counterpart

of MS is observed in a pair of coupled quantum kicked Harper chains [31], where coupling transpires between two spin chains through a potential that varies with time and site [32]. Besides, MS has been investigated in a two-species bosonic Josephson junction [11], another example of many-body quantum systems. This two-species bosonic Josephson junction can be regarded as a composite of two interlinked single-species bosonic Josephson junctions [33]. Many-body quantum problems encompass a broad class of physical inquiries concerning the attributes of microscopic systems composed of numerous interacting particles [34, 35]. This domain incorporates a diverse range of problems that hold fundamental significance in fields like chemistry, physics, and materials science [34, 35].

The Fermi-Pasta-Ulam-Tsingou (FPUT) problem is a seminal nonlinear dynamics and statistical mechanics puzzle [36, 37]. Fermi, Pasta, Ulam, and Tsingou conducted numerical simulations on a chain of particles connected by nonlinear springs. They aimed to understand how energy distributes among different vibrational modes in that one-dimensional chain. They anticipated that energy would spread among the modes equitably, a concept known as equipartition. However, they observed a phenomenon termed ‘recurrence’, wherein the system returns remarkably close to its initial state after a certain period of time. This unexpected behaviour challenged established notions about energy dissipation and highlighted the intricate and surprising dynamics that can emerge in many-body nonlinear systems.

Besides, Kuramoto and Battogtokh [38] reported an important phenomenon in 2002. A population of identical phase oscillators arranged in a ring-like geometry and subjected to a nonlocal coupling. It has been ascertained that the population is divided into two distinct subgroups of oscillators: one displaying synchrony and the other manifesting desynchrony. In other words, a symmetry breaking can transpire and lead to the emergence of desynchronous behaviour from a state of complete synchrony among identical oscillators. This study [38] sparked considerable astonishment within the nonlinear dynamics community. Anyway, an intriguing state is observed where some subsystems achieve coherence while others have certain degrees of incoherency.

Partial synchronization [39], also known as cluster [40] (or group [41]) synchronization, characterizes a phenomenon in which some, but not all, components within a system exhibit identical behaviour. An illustrative instance of partial synchronization manifests in the form of chimera states [42], which represent states of asymmetric coherence and incoherence within the system’s dynamics. In practical scenarios, chimera states find relevance in phenomena like the unihemispheric sleep patterns [43] of birds and dolphins, where one hemisphere slumbers while the other remains alert. The adjustment of inter-hemispheric coupling leads to an intermediate state of incoherence in one hemisphere, giving rise to a chimera-like partial synchronization pattern [39]. Spontaneous occurrences of chimera states have also been noted in populations of interconnected photosensitive chemical oscillators [44]. Similarly, investigations on partial synchronization states extend to diverse networked systems, including epileptic seizures [45], power grids [46], and social systems [47].

Here, we are interested in studying partial synchronization in coupled Hamiltonian systems. The partial MS [18] can be observed in systems where there are more than two subsystems coupled appropriately, for example, in systems with three subsystems. Specifically, it has been observed that the first subsystem may be in a synchronized state with the third subsystem but not with the second subsystem. This phenomenon is referred to as partial MS [17, 19]. Wang et al. [18] conduct an investigation on partial MS in the Bambi, Baowen, and Hong model [48], which serves as a representation of heat conduction in one-dimensional non-integrable systems. A transition from the partial MS state to the complete MS state has been studied for three coupled double-well Duffing Hamiltonian systems [17]. Employing both frequency-based and wavelet-based analyses, the partial MS has also been scrutinized in the presence of nonlinear coupling in the classical SU(2) Yang-Mills-Higgs Hamiltonian system [49], which has three degrees of freedom [19]. In a recent paper [27], partial MS has been studied in a network consisting of two populations of coupled metronome systems. This system encompasses numerous identical metronomes arranged on two swing boards interconnected by a spring, each representing an individual population.

This study uses the classical ϕ^4 -system to scrutinize partial MS. In Sec. 3.1, we have used the ϕ^4 -system to study the MS transition. Our approach encompasses the nearest neighbour diffusive coupling and implements the periodic boundary conditions. The Hamiltonian governing the system is as follows:

$$H = \frac{p_j^2}{2} + \frac{q_j^4}{4} + \frac{K}{2} (q_{j+1} - q_j)^2, \quad (19)$$

where $j = 1, 2, \dots, N$. The dynamics of the j^{th} oscillator is precisely determined through the following canonical equations:

$$\dot{q}_j = p_j, \quad (20a)$$

$$\dot{p}_j = -q_j^3 + K(q_{j+1} + q_{j-1} - 2q_j). \quad (20b)$$

The implementation of periodic boundary condition requires $q_{N+1} = q_1$ and $q_0 = q_N$.

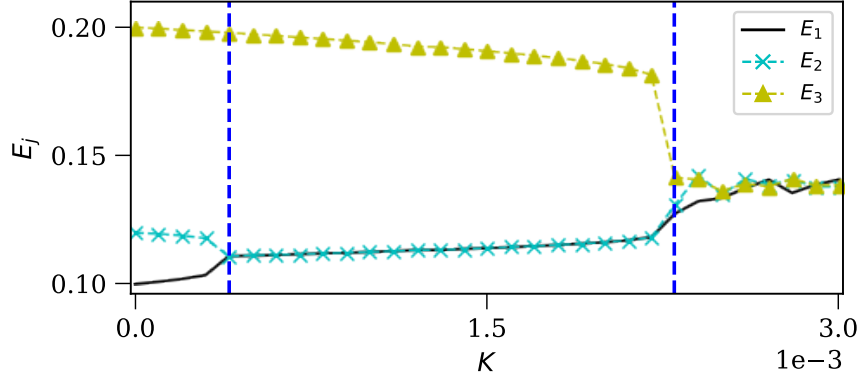


Figure 6: The average bare energies (E_j) for Eq. 20 are calculated as a function of K using Eq. 12. Two vertical blue dashed lines correspond to $K = 0.4 \times 10^{-3}$ and 2.3×10^{-3} .

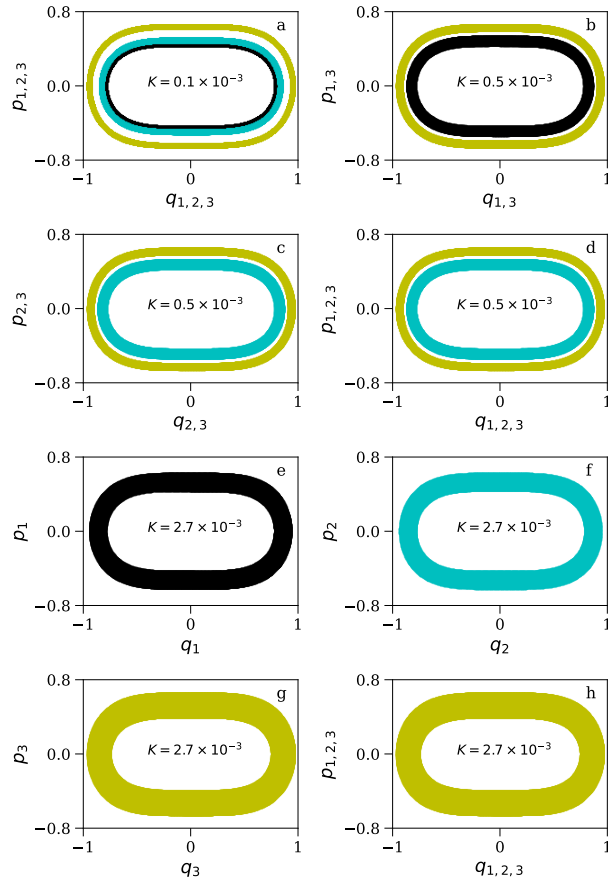


Figure 7: The black, cyan, and yellow colours correspond to the first, second, and third oscillators of Eq. 20. Subplot (a) depicts that all three oscillators are in the desynchronized state at $K = 0.1 \times 10^{-3}$. Subplots (b)–(d) describe that the first and second oscillators are in MS state at $K = 0.5 \times 10^{-3}$. However, none of them is in MS state with the third one. Subplots (e)–(h) show that all three oscillators are in MS state at $K = 2.7 \times 10^{-3}$.

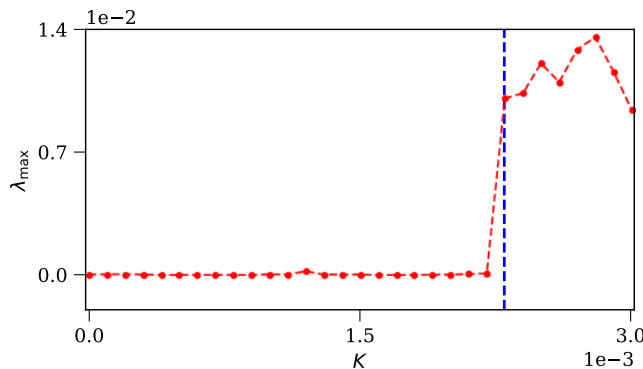


Figure 8: The maximum Lyapunov exponent (λ_{\max}) of Eq. 20 is plotted as a function of K . The vertical blue dashed line correspond to $K = 2.3 \times 10^{-3}$. A transition from quasiperiodic to chaotic dynamics is detected at the aforesaid value of K .

However, here, we adopt three oscillators (i.e., $N = 3$ in Eq. 20) and initial condition $(q_1(0), q_2(0), q_3(0), p_1(0), p_2(0), p_3(0)) = (0.0, 0.0, 0.0, \sqrt{0.2}, \sqrt{0.24}, \sqrt{0.4})$ [18]. Figure 6 depicts the variation of average bare energies (E_j) of Eq. 20 as a function of K . These average energies have been calculated using Eq. 12. For small values of K ($K < 0.4 \times 10^{-3}$), all three oscillators exhibit distinct E_j values, indicating a desynchronized state. A notable observation that distinguishes this scenario from the $N = 2$ case is that within the interval $0.4 \times 10^{-3} < K < 2.3 \times 10^{-3}$, we encounter a situation where $E_1 = E_2 \neq E_3$. This suggests that oscillators corresponding to $j = 1$ and 2 may achieve MS, while oscillator associated with $j = 3$ remains desynchronized. Consequently, due to its dynamic evolution, the system undergoes a state known as partial MS. Upon further increasing K beyond $K = 2.3 \times 10^{-3}$, we observe complete MS among all three oscillators. In order to confirm the MS state, we have plotted the projected phase portraits in two-dimensional phase space at different values of K in Fig. 7. The colours denoting the first, second, and third oscillators of Eq. 20 are as follows: black, cyan, and yellow, respectively. In Fig. 7a, it is illustrated that, at $K = 0.1 \times 10^{-3}$, all three oscillators exist in a desynchronized state. Figures 7b–7d delineate a scenario where the first and second oscillators are concurrently in the MS state at $K = 0.5 \times 10^{-3}$; however, neither of them reaches the MS state concurrently with the third oscillator. More explicitly, Fig. 7b depicts the sharing of non-overlapping phase space regions of the first and third oscillators. A similar sharing of non-overlapping areas between the second and third oscillators is depicted in Fig. 7c. Finally, in Fig. 7d, the cyan plot completely covers the black plot and yields the occurrence of MS state between the first and second oscillators; however, the yellow plot shares non-overlapping regions and yields the desynchronized state of the third oscillator with both first and second oscillators. Figures 7e–7h present a condition wherein all three oscillators simultaneously occupy a MS state at $K = 2.7 \times 10^{-3}$. In conclusion, the first and second oscillators yield the MS state at $K = 0.4 \times 10^{-3}$, while all three oscillators reach the MS state for $K \geq 2.3 \times 10^{-3}$.

This transition from desynchronization to MS is closely linked to a distinct shift in the system's dynamical behaviour. Figure 8 presents the maximum Lyapunov exponent (λ_{\max}) of the system plotted against K . A non-zero value of λ_{\max} is detected when $K \geq 2.3 \times 10^{-3}$. Therefore, a transition from quasiperiodicity to chaos coincides precisely with the turning point from partial MS to complete MS.

Now, we extend our analysis to four oscillators (i.e., $N = 4$ in Eq. 20) and adopt the initial condition $(q_1(0), q_2(0), q_3(0), q_4(0), p_1(0), p_2(0), p_3(0), p_4(0)) = (0.0, 0.0, 0.0, 0.0, \sqrt{0.2}, -\sqrt{0.42}, -\sqrt{0.24}, \sqrt{0.39})$ [18]. We observe four distinct configurations in various coupling strength regions (Fig. 9a). When K is less than 1.5×10^{-3} , the average energies of the four oscillators remain distinctly separate, resulting in a desynchronized state. Within the range $1.5 \times 10^{-3} < K < 4.5 \times 10^{-3}$, a partial MS state manifests. In this state, a pair of oscillators, i.e., oscillators corresponding to $j = 2$ and 4 , exhibit synchronization, while the other two oscillators, $j = 1$ and 3 , remain desynchronized. As K is further increased, within the $4.5 \times 10^{-3} < K < 8 \times 10^{-3}$ range, the remaining two oscillators achieve MS, leading to a distinct partial MS state characterized by a higher degree of synchronization. Remarkably, in both regions, $1.5 \times 10^{-3} < K < 4.5 \times 10^{-3}$ and $4.5 \times 10^{-3} < K < 8 \times 10^{-3}$, a noteworthy feature of nonlocal synchronization emerges. This phenomenon is akin to the behaviour observed in dissipative systems [50], where two oscillators that are not adjacent in the sequence can exhibit MS. In contrast, the intermediate oscillators remain desynchronized from them. Notably, this measure-symmetry in the nonlocal sites is not inherent in the initial conditions but rather emerges dynamically under specific suitable coupling conditions. All four oscillators attain full MS for

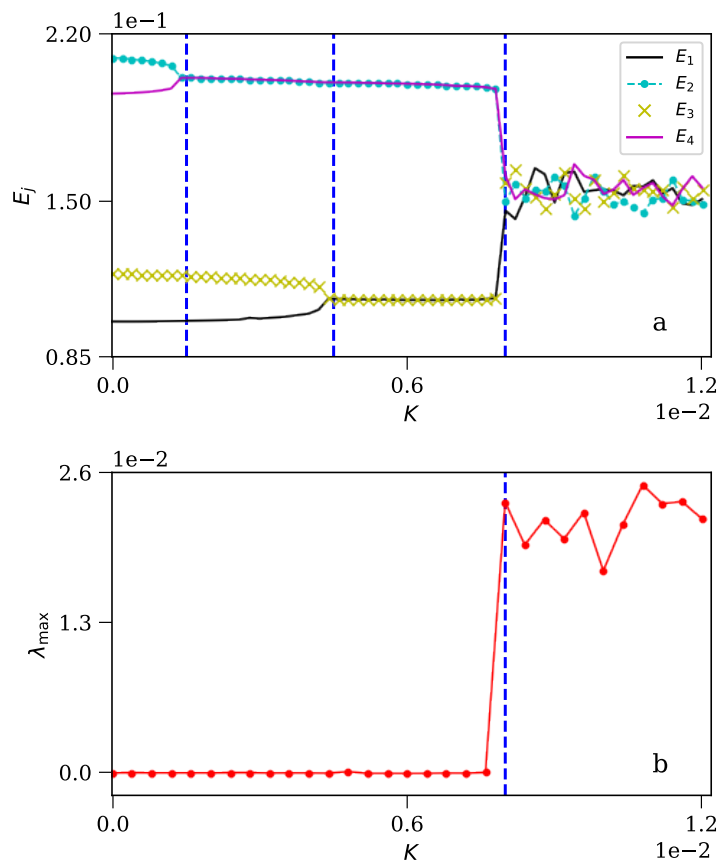


Figure 9: (a) The average bare energies (E_j) for four coupled ϕ^4 -systems, following Eq. 20, are calculated as a function of K using Eq. 12. Three vertical blue dashed lines (from left) correspond to $K = 1.5 \times 10^{-3}$, 4.5×10^{-3} and 8×10^{-3} . (b) The variation of λ_{\max} as a function of K implies a transition from quasiperiodic to chaotic dynamics is ascertained at $K = 8 \times 10^{-3}$.

sufficiently large coupling values ($K > 8 \times 10^{-3}$). Here, we have $E_1 = E_2 = E_3 = E_4$, which infers that four oscillators constitute a complete MS state.

In Fig. 9b, we observe the relationship between the maximum Lyapunov exponent, λ_{\max} , and the coupling strength K . It is clearly visible that λ_{\max} becomes positive for $K \geq 8 \times 10^{-3}$ and remains zero before this threshold. Once more, we observe a consistent pattern where the shift from quasiperiodicity to chaos coincides with the transition from partial MS to complete MS, akin to the observation in Fig. 8 for the case where $N = 3$. It is noteworthy to emphasize that chaos consistently manifests whenever complete MS occurs among nonlinear oscillators for $N \geq 3$ [18, 15].

5 Effects of occasional coupling

In interacting dynamical systems, coupling between subsystems is a fundamental prerequisite for observing synchronization [1]. While this phenomenon was initially discovered in the seventeenth-century [1], the popularity of synchronization in coupled chaotic systems grew notably after the work by Pecora and Carroll [51]. Subsequently, one of the most intriguing concepts introduced in this domain is that of ‘occasional coupling’ [52]. In this framework, the participating subsystems interact intermittently rather than continuously, and synchronization is successfully achieved. It is worth highlighting that, in many instances, occasional coupling yields robust synchronization, even in situations where continuous coupling proves inadequate. In other words, two or more initially desynchronized interacting chaotic systems attain a synchronized state when subjected to occasional coupling pulses [53].

This occasional (or intermittent) interaction can assume either a deterministic or stochastic nature [53]. For example, in the stochastic on-off coupling scheme [54], the activation or deactivation of the coupling term occurs randomly.

In contrast, the interaction follows a deterministic pattern in the on-off coupling scheme [55]. The concept of intermittent coupling has been extended to complex networks incorporating delayed coupling for the examination of synchronization [56]. Employing the occasional coupling, it is possible to render a non-synchronizable network synchronizable [57]. In multi-layered complex networks, investigations on synchronization have incorporated using time-varying inter-layer links [58]. In circadian oscillators within individual cells of fungal systems, stochastic intermittent coupling has been employed to investigate synchronization [59]. Additionally, it has been reported that periodically time-varying changes in coupling among neuron oscillators can enhance synchronization [60]. In passing, beyond the purview of synchronization, the occasional coupling is equally effective in reaching the amplitude death in coupled dynamical systems when the continuous coupling fails [61, 62].

The success of an occasional coupling scheme in inducing synchronization in dissipative chaotic systems does not necessarily guarantee its efficacy when employed on previously measure desynchronized systems. This is because occasional coupling in dissipative systems is typically ad hoc, and analytical tools such as conditional Lyapunov exponents [63] and eigenvalues of the Jacobian matrix of the corresponding linearized transverse dynamics [64] are not applicable for characterizing MS. However, the occasional coupling has found application in mitigating measure desynchronization observed in coupled Hamiltonian systems [23]. More explicitly, the use of the on-off coupling scheme [55] can effectively overcome desynchronization and restore MS between two coupled subsystems [23]. This study [23] encompasses both categories of MS states: quasiperiodic and chaotic. This paper undertakes an examination by selecting representative systems from each category and emphasizes the effect of the on-off coupling to retain the MS states in these systems.

In this on-off coupling scheme [55], the coupling parameter is periodically turned on and off at predetermined intervals. Thus, in the presence of occasional coupling, we need to take care of two time scales: the system time scale (T_s) and on-off period (T). In order to facilitate a more comprehensive discussion and to provide a clear mathematical representation of the implementation of the on-off coupling scheme [55], we express the bidirectional coupling between the two Hamiltonian subsystems using the coupling strength K in the following manner [23]:

$$\dot{\mathbf{x}} = \mathbf{f}(\mathbf{x}) + \chi(t)K\mathbf{C} \cdot \mathbf{g}(\mathbf{x}), \quad (21)$$

where

$$\chi(t) = \begin{cases} 1 & \text{for } nT \leq t < (n + \theta)T, \\ 0 & \text{for } (n + \theta)T \leq t < (n + 1)T, \end{cases} \quad (22)$$

and θ is the on-off fraction. By definition, $\theta = 0$ and 1 refer to the cases when the coupling is inactive, and the continuous coupling is activated between the oscillators, respectively. Hence, the value of θ must lie between 0 and 1 , i.e. $0 < \theta < 1$, to keep the occasional coupling activated. Following Eq. 11 and Eq. 21, we have $\mathbf{x} = (q_1, q_2, p_1, p_2)$, $\mathbf{f}(\mathbf{x}) = (p_1, p_2, -q_1^3, -q_2^3)$, and $\mathbf{g}(\mathbf{x}) = (0, 0, 2q_2 - 2q_1, -2q_2 + 2q_1)$. In addition, $K = K_Q$ and the coupling matrix $\mathbf{C}_{mn} = \delta_{m3}\delta_{n3} + \delta_{m4}\delta_{n4}$, where δ is the Kronecker delta. Similarly, one can easily connect Eq. 18 with Eq. 21 and define associated column vectors \mathbf{x} , $\mathbf{f}(\mathbf{x})$, and $\mathbf{g}(\mathbf{x})$ and the coupling matrix \mathbf{C} .

The solution of Eq. 21 can be written as:

$$\mathbf{x}(t+T) = \mathbf{x}(t) + \int_t^{t+T} \mathbf{f}(\mathbf{x}(t')) dt' + \int_t^{t+T} \chi(t')K\mathbf{C} \cdot \mathbf{g}(\mathbf{x}(t')) dt'. \quad (23)$$

If T is significantly smaller than the system time-scale (T_s), the functions \mathbf{f} and \mathbf{g} do not vary much and can be considered constant over the time T . Therefore, in the presence of the assumption that \mathbf{f} and \mathbf{g} remain constant throughout the time interval T , we can approximately write $\mathbf{x}(t+T)$ as follows:

$$\mathbf{x}(t+T) \approx \mathbf{x}(t) + \mathbf{f}(\mathbf{x}(t))T + \theta K\mathbf{C} \cdot \mathbf{g}(\mathbf{x}(t))T. \quad (24)$$

In the last term, we have explicitly integrated the concept that the coupling operates solely during a fraction θ of the total time T . Consequently, it becomes evident that we can conceptualize the system subject to the on-off coupling as equivalent to the system subjected to continuous coupling, albeit with an effectively reduced coupling strength value, denoted as follows:

$$K_{\text{eff}} = \theta K. \quad (25)$$

Therefore, for the condition $T \ll T_s$, a linear stability analysis has been performed for coupled oscillators and analytically understand the shifting of the desynchronized window along the higher range of coupling strength [23]. Although this approximate connection of the on-off coupling and the continuous coupling schemes is inapplicable for $T \sim T_s$, the on-off coupling scheme can lead to MS for $T \sim T_s$ [23]. Besides, the effectiveness of the transient uncoupling scheme, another example of the occasional coupling scheme, has also been reported in the literature to attain MS when the continuous coupling fails [23]. A general understanding of why and how these occasional coupling schemes work is still missing in the literature.

In a subsequent study [65], the occasional coupling has been used to investigate MS in a two-species bosonic Josephson junction. This study reveals that the broken symmetry of nonlocal MS states appearing in the 0-phase mode and π -phase mode can be restored by employing the on-off coupling scheme. It has also demonstrated that the nonlocal MS states can be transformed into conventional MS states, either quasiperiodic or chaotic MS states. More specifically, for the 0-phase mode, the broken symmetry restores by converting the nonlocal MS state into a conventional quasiperiodic MS state. However, for the π -phase mode, the broken symmetry is restored, and chaotic MS states emerge.

Until now, we have kept ourselves restrictive in the classical regime. MS in quantum systems has also been the subject of extensive research over the last decade, focusing on understanding its fundamental properties and exploring its potential applications in areas such as quantum information processing and quantum communication.

6 MS in quantum systems

The underlying principle of the MS is rooted in the notion of the area enclosed by the trajectory in phase space. However, this concept of phase space is not applicable in quantum mechanics. Consequently, one cannot apply the concept of the MS directly to quantum systems, but its equivalent can be observed. This section studies the transition to MS in a two-species bosonic Josephson junction (BJJ). From an experimental perspective, the superconducting Josephson junction has emerged as one of the extensively investigated systems in the exploration of synchronization. This specific junction stands as a prominent model of coupled dynamical systems. Moreover, recent advancements in the experimental manipulation of Bose-Einstein condensation have facilitated the creation and control of a BJJ [66]. A two-species BJJ can be achieved experimentally by confinement of a binary mixture of Bose-Einstein condensations within a symmetric double-well potential. In a seminal theoretical investigation, Smerzi et al. [33] have established a mapping between a single-species BJJ and a classical pendulum system. In this section, MS is studied in a two-species BJJ based on semiclassical [10] and quantum [11] approaches in Sec. 6.1 and Sec. 6.2, respectively.

6.1 MS using semiclassical approach

Tian et al. [10] have studied MS in quantum systems using a semiclassical approach under the assumption of sufficiently weak interatomic interactions and employing the established two-mode approximation [67]. The corresponding Hamiltonian in the second quantization is expressed as follows:

$$\begin{aligned} \hat{H} = & \frac{u_1}{2N_1} \left[(\hat{a}_L^\dagger \hat{a}_L)^2 + (\hat{a}_R^\dagger \hat{a}_R)^2 \right] + \frac{u_2}{2N_2} \left[(\hat{b}_L^\dagger \hat{b}_L)^2 + (\hat{b}_R^\dagger \hat{b}_R)^2 \right] - \frac{v_1}{2} (\hat{a}_L^\dagger \hat{a}_R + \hat{a}_R^\dagger \hat{a}_L) - \frac{v_2}{2} (\hat{b}_L^\dagger \hat{b}_R + \hat{b}_R^\dagger \hat{b}_L) \\ & + \frac{u_{12}}{\sqrt{N_1 N_2}} (\hat{a}_L^\dagger \hat{a}_L \hat{b}_L^\dagger \hat{b}_L + \hat{a}_R^\dagger \hat{a}_R \hat{b}_R^\dagger \hat{b}_R), \end{aligned} \quad (26)$$

where \hat{a}_R and \hat{a}_L are the annihilation operators correspond to the localized modes in the right and left wells, respectively, of the first species a with the total number of particles N_1 . Similarly, \hat{a}_R^\dagger and \hat{a}_L^\dagger are the respective creation operators corresponding to right and left wells of the first species. The second species b , consists of total N_2 particles, has annihilation (creation) operators \hat{b}_R (\hat{b}_R^\dagger) and \hat{b}_L (\hat{b}_L^\dagger) for the right and left wells, respectively. The parameters u_i (where $i = 1, 2$) and u_{12} represent the effective interaction strengths associated with atomic collisions involving species of the same kind and species of different kinds, respectively. Finally, v_i , the effective Rabi frequency, measures the interaction strength between two wells.

In the semiclassical regime [33, 68, 67], the evolution of the system can be characterized through a classical Hamiltonian denoted as $H = \langle \Psi | \hat{H} | \Psi \rangle$, where $|\Psi\rangle = \frac{1}{\sqrt{N_1}} (\alpha_L \hat{a}_L^\dagger + \alpha_R \hat{a}_R^\dagger)^{N_1} |0, 0\rangle \otimes \frac{1}{\sqrt{N_2}} (\beta_L \hat{b}_L^\dagger + \beta_R \hat{b}_R^\dagger)^{N_2} |0, 0\rangle$ is a collective state with total number of particles $N = N_1 + N_2$. In this context, four c numbers, $\alpha_L = |\alpha_L| e^{i\theta_{1L}}$, $\alpha_R = |\alpha_R| e^{i\theta_{1R}}$, $\beta_L = |\beta_L| e^{i\theta_{2L}}$, and $\beta_R = |\beta_R| e^{i\theta_{2R}}$, represent the probability amplitudes associated with the presence of two distinct species of atoms within the two wells. The conservation of particle numbers for each species mandates that $|\alpha_L|^2 + |\alpha_R|^2 = 1$ and $|\beta_L|^2 + |\beta_R|^2 = 1$. Upon the introduction of the relative population differences, denoted as $S_1 = (|\alpha_L|^2 - |\alpha_R|^2)$ and $S_2 = (|\beta_L|^2 - |\beta_R|^2)$, along with the relative phase differences $\theta_1 = (\theta_{1L} - \theta_{1R})$ and $\theta_2 = (\theta_{2L} - \theta_{2R})$, we derive the mean-field Hamiltonian as presented below:

$$H = H_1(\theta_1, S_1) + H_2(\theta_2, S_2) + H_c, \quad (27)$$

where

$$H_i(\theta_i, S_i) = -\frac{u_i}{2} S_i^2 + v_i \sqrt{1 - S_i^2} \cos \theta_i, \quad (28)$$

and

$$H_c = -u_{12} S_1 S_2. \quad (29)$$

Therefore, a two-species BJJ exhibits similarities to two interlinked single-species BJJs. It is evident that the coupling arises due to the interspecies interaction u_{12} . The equations of motion can be deduced as follows:

$$\dot{\theta}_1 = -u_1 S_1 - \frac{v_1 S_1}{\sqrt{1-S_1^2}} \cos \theta_1 - u_{12} S_2, \quad (30a)$$

$$\dot{S}_1 = v_1 \sqrt{1-S_1^2} \sin \theta_1, \quad (30b)$$

$$\dot{\theta}_2 = -u_2 S_2 - \frac{v_2 S_2}{\sqrt{1-S_2^2}} \cos \theta_2 - u_{12} S_1, \quad (30c)$$

$$\dot{S}_2 = v_2 \sqrt{1-S_2^2} \sin \theta_2. \quad (30d)$$

As our focus lies in illustrating the influence of coupling on the dynamics of each species, we represent the collective motion by projecting the state of the complete system onto the respective individual phase spaces. We adopt the parameter values $u_1 = u_2 = 1.2$ and $v_1 = v_2 = 1$, and the initial condition $(\theta_1(0), S_1(0)), (\theta_2(0), S_2(0)) = (0.0, 0.2, 0.0, 0.4)$ [10]. To this end, following Eq. 12, we can define the average energy of each single-species BJJ as follows:

$$E_i = \frac{1}{T_f} \int_0^{T_f} H_i(\theta_i, S_i) dt. \quad (31)$$

Figures 10b and 10c depict the temporal evolution of MS under the influence of repulsive interspecies interactions (i.e., $u_{12} > 0$). As the coupling strength u_{12} is monotonically increased, we trace the trajectories on the (θ_i, S_i) phase plane for the two subsystems. For $u_{12} = 0$, as illustrated in Fig. 10a, the initial conditions correspond to two distinct quasiperiodic orbits, forming enclosed curves. However, as u_{12} is raised above zero, these two enclosed curves transform into smooth quasiperiodic trajectories that meander within separate phase-space regions, adopting a ring-like shape. With the continued increase in u_{12} , the two phase-space regions undergo a gradual transformation, wherein the outer boundary of the inner domain approaches the inner boundary of the outer domain. They draw nearer to each other until u_{12} reaches a critical value of 8.6×10^{-4} , as depicted in Fig. 10b, at which point the two converging boundaries nearly touch. Beyond this threshold $u_{12} = 8.6 \times 10^{-4}$, the MS state between these two species a and b is detected, as exemplified in Fig. 10c. The previously distinct phase-space domains, formally well-separated, converge and envelop the phase-space regions with indistinguishable invariant measures.

Figures 10d and 10e portray the progression with increasing strength of attractive interspecies interactions. We again start with Fig. 10a when no coupling is activated. For values of u_{12} less than zero (i.e., $u_{12} < 0$), we can also reach MS from the initial desynchronized state. Non-overlapping ring-like bands are detected at $u_{12} = -0.06$ (Fig. 10d). Finally, MS has been detected at $u_{12} = -0.08$ (Fig. 10e). Note that routes to MS are different for attractive and repulsive interspecies interactions [10]. In Fig. 10f, we present the average energies E_1 and E_2 as functions of the interspecies interactions denoted by u_{12} . Notably, distinct sharp transitions occur at $u_{12} = -7.38 \times 10^{-3}$ and $u_{12} = 8.6 \times 10^{-4}$ for the cases of repulsive and attractive interactions, respectively. These two transition points are shown using two verticle blue dashed lines in Fig. 10f. A finite disparity between E_1 and E_2 is evident when the value of u_{12} lies within the region bounded by the blue verticle dashed lines. Conversely, both species exhibit identical average energies when the value of u_{12} remains outside the aforesaid boundary.

The semiclassical theory has revealed the existence of two distinct dynamic regimes [33, 68, 69] of a single-species BJJ: the Josephson oscillation regime and the self-trapping regime. In our discussion, we have examined MS in the Josephson oscillation regime, where the variable θ_i oscillates in proximity to $\theta_i = 0$, signifying the zero-phase mode. However, it is noteworthy that MS has also been observed in the self-trapping regime [10], where θ_i undergoes oscillations around $\theta_i = \pi$, corresponding to the π -phase mode. Six different scenarios of MS, including two in the 0-phase mode (Fig. 10) and four in the localized and nonlocalized π -phase modes, are characterized, and common features behind them are revealed. The MS transition corresponds to the sudden merger of the average energies of the two species. The power law scaling with a critical exponent of $1/2$ is verified for all scenarios. Moreover, a three-dimensional view of MS is provided, revealing features that are not visible in the two-dimensional phase space. Poincaré section analysis shows that a two-species bosonic Josephson junction exhibits separatrix crossing behaviour at the critical coupling intensity. It is concluded that separatrix crossing is the general mechanism underlying the different scenarios of MS transitions in the two-species bosonic Josephson junction. In the case of MS transition from quasiperiodic to quasiperiodic dynamics, the maximum Lyapunov exponent (λ_{\max}) of the Hamiltonian system is positive at the transition point (the point of separatrix crossing) [20]. However, this point is singular and unmeasurable [20].

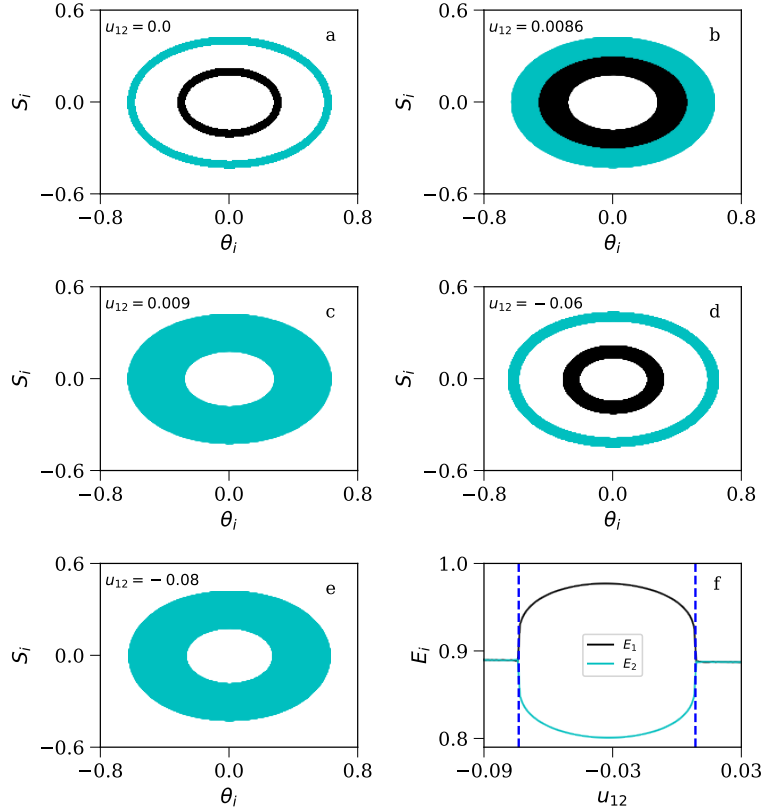


Figure 10: The black and cyan colours correspond to the first and second oscillators of Eq. 30. Subplot (a) represents phase space diagram when no interspecies interaction is activated. Transition to MS is studied in the presence of repulsive (subplots (b) and (c)) and attractive (subplots (d) and (e)) interspecies interactions. The average energies of each species are plotted as a function of the interspecies interaction u_{12} in subplot (f). The vertical blue dashed lines correspond to -7.38×10^{-3} and $u_{12} = 8.6 \times 10^{-4}$.

6.2 MS using quantum approach

A close analogy of MS in quantum scenario has been made by Qiu et al [11]. They have characterized the quantum many-body MS in a three-dimensional (3D) space defined by the average value of the pseudoangular momentum. The dynamics of two quantum many-body systems become coupled through particle-particle interactions. The Hamiltonian of a two-species BJJ can be written as follows:

$$\hat{H} = \hat{H}_1 + \hat{H}_2 + \hat{H}_{12}, \quad (32)$$

where

$$\begin{aligned} \hat{H}_1 &= \frac{u_1}{2} \left[(\hat{a}_L^\dagger \hat{a}_L)^2 + (\hat{a}_R^\dagger \hat{a}_R)^2 \right] - v_1 (\hat{a}_L^\dagger \hat{a}_R + \hat{a}_R^\dagger \hat{a}_L), \\ \hat{H}_2 &= \frac{u_2}{2} \left[(\hat{b}_L^\dagger \hat{b}_L)^2 + (\hat{b}_R^\dagger \hat{b}_R)^2 \right] - v_2 (\hat{b}_L^\dagger \hat{b}_R + \hat{b}_R^\dagger \hat{b}_L), \\ \hat{H}_{12} &= u_{12} (\hat{a}_L^\dagger \hat{a}_L \hat{b}_L^\dagger \hat{b}_L + \hat{a}_R^\dagger \hat{a}_R \hat{b}_R^\dagger \hat{b}_R). \end{aligned}$$

The Hamiltonian under consideration (Eq. 32) can be subjected to numerical diagonalization within the $N_d = (N_1 + 1)(N_2 + 1)$ dimensional space, defined by the tensor product of the many-body Fock basis $|N_{1,L}\rangle$ and $|N_{2,L}\rangle$ spanning the a and b Fock states, where $N_{1,L} = 0, 1, \dots, N_1$ and $N_{2,L} = 0, 1, \dots, N_2$. A general N -particle state can be expressed as

$$|\Psi\rangle = \sum_{N_{1,L}=0}^{N_1} \sum_{N_{2,L}=0}^{N_2} c_{N_{1,L}, N_{2,L}} |N_{1,L}, N_{2,L}\rangle \quad (33)$$

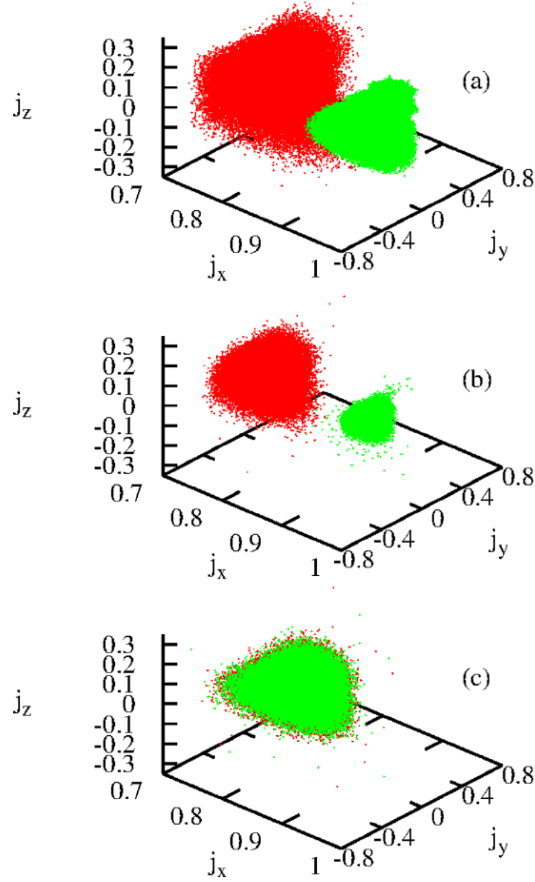


Figure 11: MS in many-body quantum system is distinguished by the region traversed by each subsystem during its evolution in the 3D space characterized by the average pseudoangular momentum $j_x = (2/N) \langle \hat{J}_x \rangle$, $j_y = (2/N) \langle \hat{J}_y \rangle$, and $j_z = (2/N) \langle \hat{J}_z \rangle$. The red and green colours correspond to species a and b , respectively. Specifically, for the initial conditions $Z_1(0) = 0.2$, $Z_2(0) = 0.4$, and $N_1 = N_2 = 30$, we observe the following scenarios: (a) When $u_{12} = 0$ (desynchronization), (b) When $u_{12} = 0.008u$ (desynchronization), and (c) When $u_{12} = 0.5u$ (MS). In subplot (c), the two clouds representing the subsystems exhibit substantial overlap. This figure is taken from Qiu et al. [11] with permission.

The time-dependent Schrödinger equation determines the temporal evolution of any initial state. We can deduce the average particle numbers $\langle N_{1,\alpha} \rangle = \langle \Psi | \hat{a}_\alpha^\dagger \hat{a}_\alpha | \Psi \rangle$ and $\langle N_{2,\alpha} \rangle = \langle \Psi | \hat{b}_\alpha^\dagger \hat{b}_\alpha | \Psi \rangle$ (where $\alpha = L, R$) associated with the L and R modes upon computing the many-body state. The population imbalance for each species is quantified as $Z_{1(2)} = (N_{1(2),L} - N_{1(2),R}) / N_{1(2)}$. To characterize the extent of condensation within each subsystem, a and b , we employ the one-body density matrix ρ [70]. The traces of ρ_1 and ρ_2 are normalized to the number of atoms in each respective subsystem, denoted as N_1 and N_2 .

We establish equivalent intraspecies interactions, specifically $u = u_1 = u_2$, with a value of $Nu/v = 7.2$, and equivalent linear couplings, denoted as $v_1 = v_2 = v$. We utilize the Rabi time, $t_{Rabi} = \pi/v$, as our unit of time, and \hbar/t_{Rabi} as our unit of energy. Our initial states consistently assume the form of coherent states for both species a and b , where all atoms occupy the single-particle state $(1/\sqrt{2}) (\cos(\theta/2) \hat{a}_L^\dagger + \sin(\theta/2) \hat{a}_R^\dagger)$. The transition from desynchronization to MS state is graphically depicted in Fig. 11. We plot the mean values of the pseudoangular momentum operators, $\hat{J}_x = (1/2) (\hat{a}_L^\dagger \hat{a}_R + \hat{a}_L \hat{a}_R^\dagger)$, $\hat{J}_y = (1/2) (\hat{a}_L^\dagger \hat{a}_R - \hat{a}_L \hat{a}_R^\dagger)$, and $\hat{J}_z = (1/2) (\hat{a}_L^\dagger \hat{a}_L - \hat{a}_R^\dagger \hat{a}_R)$, which can be readily constructed from the creation and annihilation operators of each species. As evidenced in the 3D representation, in the instances of desynchronized dynamics, i.e., when $u_{12} = 0$ (Fig. 11a) and $u_{12} = 0.008u$ (Fig. 11b), the domains

explored by each subsystem in the $(\langle \hat{J}_x \rangle, \langle \hat{J}_y \rangle, \langle \hat{J}_z \rangle)$ space remain disjointed. In contrast, in the MS case (Fig. 11c), both domains exhibit complete overlap. This characteristic can be interpreted as the many-body counterpart of the classical definition of MS, wherein the phase space domain covered by both subsystems coincides. To this end, a method for quantifying the transition from desynchronization to MS dynamics in classical systems involves examining the time-averaged bare energies of interacting subsystems. This energy-based index (Eq. 31) equally applies to studying the transition to MS in the quantum scenario.

MS has also been investigated in a pair of coupled Harper systems in classical and quantum contexts [32]. This study demonstrates the quantum counterpart of synchronization in a pair of coupled quantum-kicked Harper chains. Two spin chains are coupled through a time and site-dependent potential. The average interaction energy between the participating systems is used as an order parameter in classical and quantum contexts to establish a connection between the scenarios. In addition, this study also examines the entanglement between the chains and the difference between the average bare energies in the quantum context. Interestingly, all indicators suggest a connection between the MS transition in classical maps and a phase transition in quantum spin chains.

Zhang et al [71] investigate the synchronization of two nonlinear mechanical modes of Bose-Einstein condensates in a closed quantum system, using classical and quantum measures. The aim is to reveal the macroscopic and microscopic properties of synchronized behaviours. The authors have used the Pearson correlation coefficient, orbital overlapping, and covering areas in the phase space based on mean-value dynamical equations to identify MS in the classical picture. On the other hand, the Husimi Q functions have been used to display the synchronized behaviours of quantum MS based on density overlapping and correlated probability dynamics in phase space. The quantum MS has been further investigated using two other quantum measures: the Mari measure and mutual information.

Another study [72] explores MS in hybrid quantum-classical systems. The dynamics of the classical subsystem are modelled by Hamiltonian equations, while the Schrödinger equation governs the dynamics of the quantum subsystem. The authors have also explained the physical reason behind MS, which is the classical-like behavior of the quantum subsystem as the coupling strength increases. This effect leads to MS in quantum scenario mimicking MS in coupled classical Hamiltonian systems. Additionally, the frequency spectra of the MS states exhibit similar results to classical MS states with increasing coupling strength.

A similar kind of synchronization, termed hybrid synchronization (HS), has been studied considering the dynamics of coupled ultracold atomic clouds after changing the coupling strength between them [12]. HS can coexist as compared to MS in the same model system. These two types of synchronizations differ in two ways. First, MS is a synchronization that occurs in the spatial coincidence sense and is characterized by a unique synchronization with an invariant measure in the phase space domain [9]. Conversely, HS is a synchronization that occurs in the time coincidence sense and is a general term for synchronization that is characterized by strong time correlation in coupled quantum-classical dynamics. The time correlation in HS can be as strong as complete synchronization [6] in coupled dissipative systems, while in terms of time correlation, MS is much weaker. Secondly, there are significant differences in setting the initial conditions and parameters for HS and MS. For HS, the quantum and classical subsystems must have initial conditions with exact correspondence. In contrast, the initial conditions cannot have exact correspondence and must be different in the case of MS.

7 Conclusion and discussions

In conclusion, we have comprehended MS in interacting Hamiltonian systems in this paper. Each system shares a phase space domain with an identical invariant measure in the MS state. This kind of synchronization is observed when the Hamiltonian systems exhibit either quasiperiodic or chaotic dynamics. Although synchronization in dynamical systems has been a topic of intense research over the last few decades, discussions on MS needed to catch up. We have discussed MS incorporating both classical and quantum scenarios in this paper. Along with Hamiltonian systems with two interacting subsystems, studies on MS have also been extended to the many-body systems, i.e., Hamiltonian systems consisting of three or more subsystems. To this end, the notion of partial MS has been incorporated. Note that this kind of synchronization is relatively less robust than other types of synchronization observed in coupled dynamical systems.

Besides, the anticipation of synchronization is an essential aspect of studying coupled dynamical systems [73, 74]. It is well known that synchronization occurs when the coupling between the systems is strong enough to overcome the intrinsic differences in their dynamics. However, the anticipation of synchronization refers to predicting the conditions under which synchronization occurs before it happens. This can be accomplished through analytical, numerical, or experimental methods. Anticipation of synchronization is crucial for practical applications such as control and communication, where the ability to predict synchronization can aid in designing more effective control strategies

or communication protocols. Moreover, the anticipation of synchronization can provide insights into the underlying mechanisms of collective behaviour in complex systems, leading to a better understanding of the dynamics of natural and engineered systems. MS can be anticipated using a parameter-aware reservoir computing technique based on machine learning [75].

Complex network [76] is another open direction for further research on MS. Various small-world networks represent different real-life systems. Furthermore, plenty of real-world complex systems are better represented by multi-layer networks and ignoring multiplexity with other layers may result in the wrong prediction of the outcome of coupled units in one layer. In multiplex, we have to deal with two types of coupling: inter-layer and intra-layer [77]. To date, one paper [27] focuses on this topic and investigates MS in a two-population network of coupled metronomes system.

Finally, the investigation of indirectly coupled dynamical systems is of significant interest since it is a prevalent phenomenon in nature. Each dynamical system interacts with others through a common environment or medium such as air, water, and signalling chemicals. The emergence of collective behaviour in the natural world is closely related to indirect coupling. MS, as collective behaviour in Hamiltonian systems, can arise under various coupling schemes, including indirectly coupled schemes, as well as linearly and nonlinearly coupled schemes. An article [15] shows this is also the case for MS in coupled Hamiltonian systems. However, a lot needs to be uncovered in future to incorporate indirect coupling in the context of MS.

Acknowledgment

The author thanks Dr. Tirth Shah and Dr. Saikat Sur for several fruitful discussions on measure synchronization. The author also thanks anonymous referees for their comments to improve the quality of the paper. This study is supported by the Czech Science Foundation, Project No. GA24-11113S and by the Czech Academy of Sciences, Praemium Academiae awarded to Dr. M. Paluš.

References

- [1] A. Pikovsky, M. Rosenblum, and J. Kurths. *Synchronization: A Universal Concept in Nonlinear Sciences*. Cambridge University Press, New York, first edition, 2001.
- [2] A. Arenas, A. Díaz-Guilera, J. Kurths, Y. Moreno, and C. Zhou. Synchronization in complex networks. *Phys. Rep.*, 469:93, 2008. ISSN 0370-1573. doi:<https://doi.org/10.1016/j.physrep.2008.09.002>.
- [3] A. Balanov, N. Janson, D. Postnov, and O. Sosnovtseva. *Synchronization: From Simple to Complex*. Springer Press, Berlin, first edition, 2008.
- [4] A. Ghosh and R. I. Sujith. Emergence of order from chaos: A phenomenological model of coupled oscillators. *Chaos Solitons Fractals*, 141:110334, 2020. ISSN 0960-0779. doi:<https://doi.org/10.1016/j.chaos.2020.110334>.
- [5] C. Huygens. Horoloqium oscilatorium. *Apud F. Muquet, Parisiis*, 1673.
- [6] L. M. Pecora, T. L. Carroll, G. A. Johnson, D. J. Mar, and J. F. Heagy. Fundamentals of synchronization in chaotic systems, concepts, and applications. *Chaos*, 7:520, 1997. doi:10.1063/1.166278.
- [7] A. J. Lichtenberg and M. A. Leiberman. *Regular and Chaotic Dynamics*. Springer-Verlag, USA, first edition, 1992.
- [8] S. H. Strogatz. *Nonlinear Dynamics and Chaos: With Applications to Physics, Biology, Chemistry, and Engineering*. CRC Press, India, second edition, 2014.
- [9] A. Hampton and D. H. Zanette. Measure synchronization in coupled Hamiltonian systems. *Phys. Rev. Lett.*, 83: 2179, 1999. doi:10.1103/PhysRevLett.83.2179.
- [10] J. Tian, H. Qiu, G. Wang, Y. Chen, and L. Fu. Measure synchronization in a two-species bosonic Josephson junction. *Phys. Rev. E*, 88:032906, 2013. doi:10.1103/PhysRevE.88.032906.
- [11] H. Qiu, B. Juliá-Díaz, M. A. Garcia-March, and A. Polls. Measure synchronization in quantum many-body systems. *Phys. Rev. A*, 90:033603, 2014.
- [12] H. Qiu, R. Zambrini, A. Polls, J. Martorell, and B. Juliá-Díaz. Hybrid synchronization in coupled ultracold atomic gases. *Phys. Rev. A*, 92:043619, 2015.
- [13] F. Bemani, A. Motazedifard, R. Roknizadeh, M. H. Naderi, and D. Vitali. Synchronization dynamics of two nanomechanical membranes within a Fabry-Perot cavity. *Phys. Rev. A*, 96:023805, 2017.
- [14] H. Lebesgue. Intégrale, longueur, aire. *Ann. Mat. Pura Appl.*, 7:231, 1902. doi:10.1007/BF02420592.

- [15] J. Tian, B. Li, T. Liu, and H. Qiu. Measure synchronization and clustering in a coupled-pendulum system suspended from a common beam. *Chaos*, 29:093131, 2019. doi:10.1063/1.5092530.
- [16] X. Wang, M. Zhan, C. H. Lai, and H. Gang. Measure synchronization in coupled φ^4 Hamiltonian systems. *Phys. Rev. E*, 67:066215, 2003. doi:10.1103/PhysRevE.67.066215.
- [17] U. E. Vincent. Measure synchronization in coupled Duffing Hamiltonian systems. *New J. Phys.*, 7:209, 2005. doi:10.1088/1367-2630/7/1/209.
- [18] X. Wang, H. Li, K. Hu, and G. Hu. Partial measure synchronization in Hamiltonian systems. *Int. J. Bifurc. Chaos*, 12:1141, 2002. doi:10.1142/S0218127402004978.
- [19] S. De, S. Gupta, M. S. Janaki, and A. N. Sekar Iyengar. Frequency and wavelet based analyses of partial and complete measure synchronization in a system of three nonlinearly coupled oscillators. *Chaos*, 28:113108, 2018. doi:10.1063/1.5049800.
- [20] J. Tian, H. Qiu, Z. Chen, and Y. Chen. Poincaré section analysis to measure synchronization in coupled Hamiltonian systems. *Mod. Phys. Lett. B*, 27:1350036, 2013. doi:10.1142/S021798491350036X.
- [21] T. Jing, Q. Hai-Bo, and C. Yong. Nonlocal measure synchronization in coupled Bosonic Josephson junctions. *Chin. Phys. Lett.*, 27:070501, 2010. doi:10.1088/0256-307X/27/7/070501.
- [22] S. Gupta, S. De, M. S. Janaki, and A. N. Sekar Iyengar. Exploring the route to measure synchronization in non-linearly coupled Hamiltonian systems. *Chaos*, 27:113103, 2017. doi:10.1063/1.4996814.
- [23] A. Ghosh, T. Shah, and S. Chakraborty. Occasional uncoupling overcomes measure desynchronization. *Chaos*, 28:123113, 2018. doi:10.1063/1.5057436.
- [24] C. Shao-Ying, W. Guang-Rui, and C. Shi-Gang. Measure synchronization of high-cycle islets in coupled Hamiltonian systems. *Chin. Phys. Lett.*, 21:2128, 2004. doi:10.1088/0256-307X/21/11/015.
- [25] F.L. Dubeibe, A. Riaño-Doncel, and E. E. Zotos. Dynamical analysis of bounded and unbounded orbits in a generalized Hénon–Heiles system. *Phys. Lett. A*, 382:904, 2018. doi:https://doi.org/10.1016/j.physleta.2018.02.001.
- [26] U. E. Vincent, A. N. Njah, and O. Akinlade. Measure synchronization in a coupled Hamiltonian system associated with nonlinear Schrödinger equation. *Mod. Phys. Lett. B*, 19:737, 2005. doi:10.1142/S0217984905008748.
- [27] J. Tian, J. Ying, T. Qiao, and H. Qiu. Collective dynamics in multi-population Hamiltonian systems. *J. Korean Phys. Soc.*, page 1976, 2023. doi:10.1007/s40042-023-00785-y.
- [28] S. Bose. Quantum communication through an unmodulated spin chain. *Phys. Rev. Lett.*, 91:207901, 2003. doi:10.1103/PhysRevLett.91.207901.
- [29] M. Christandl, N. Datta, A. Ekert, and A. J. Landahl. Perfect state transfer in quantum spin networks. *Phys. Rev. Lett.*, 92:187902, 2004. doi:10.1103/PhysRevLett.92.187902.
- [30] V. Subrahmanyam. Entanglement dynamics and quantum-state transport in spin chains. *Phys. Rev. A*, 69:034304, 2004. doi:10.1103/PhysRevA.69.034304.
- [31] P. G. Harper. The general motion of conduction electrons in a uniform magnetic field, with application to the diamagnetism of metals. *Proc. Phys. Soc. A*, 68:879, 1955. doi:10.1088/0370-1298/68/10/305.
- [32] S. Sur and A. Ghosh. Quantum counterpart of measure synchronization: A study on a pair of Harper systems. *Phys. Lett. A*, 384:126176, 2020. ISSN 0375-9601. doi:https://doi.org/10.1016/j.physleta.2019.126176.
- [33] A. Smerzi, S. Fantoni, S. Giovanazzi, and S. R. Shenoy. Quantum coherent atomic tunneling between two trapped Bose-Einstein condensates. *Phys. Rev. Lett.*, 79:4950, 1997. doi:10.1103/PhysRevLett.79.4950.
- [34] A. Fabrocini, S. Fantoni, and E. Krotscheck. *Introduction to Modern Methods of Quantum Many-body Theory and Their Applications*. Series on advances in quantum many-body theory and their applications. World Scientific, 2002. ISBN 9789812380692.
- [35] A. L. Fetter and J. D. Walecka. *Quantum Theory of Many-particle Systems*. Dover Books on Physics. Dover Publications, 2003. ISBN 9780486428277.
- [36] J. Ford. The Fermi-Pasta-Ulam problem: Paradox turns discovery. *Phys. Rep.*, 213:271, 1992. ISSN 0370-1573. doi:https://doi.org/10.1016/0370-1573(92)90116-H.
- [37] T. Dauxois. Fermi, Pasta, Ulam, and a mysterious lady. *Phys. Today*, 61:55, 2008. ISSN 0031-9228. doi:10.1063/1.2835154.
- [38] Y. Kuramoto and D. Battogtokh. Coexistence of coherence and incoherence in nonlocally coupled phase oscillators, 2002.

- [39] E. Schöll. Partial synchronization patterns in brain networks. *EPL*, 136:18001, 2022. doi:10.1209/0295-5075/ac3b97.
- [40] L. Su, Y. Wei, W. Michiels, E. Steur, and H. Nijmeijer. Robust partial synchronization of delay-coupled networks. *Chaos*, 30:013126, 2020. doi:10.1063/1.5111745.
- [41] C. R. S. Williams, T. E. Murphy, R. Roy, F. Sorrentino, T. Dahms, and E. Schöll. Experimental observations of group synchrony in a system of chaotic optoelectronic oscillators. *Phys. Rev. Lett.*, 110:064104, 2013. doi:10.1103/PhysRevLett.110.064104.
- [42] D. M. Abrams and S. H. Strogatz. Chimera states for coupled oscillators. *Phys. Rev. Lett.*, 93:174102, 2004. doi:10.1103/PhysRevLett.93.174102.
- [43] N. C. Rattenborg, C. J. Amlaner, and S. L. Lima. Behavioral, neurophysiological and evolutionary perspectives on unihemispheric sleep. *Neurosci. Biobehav. Rev.*, 24:817, 2000. doi:https://doi.org/10.1016/S0149-7634(00)00039-7.
- [44] S. Nkomo, M. R. Tinsley, and K. Showalter. Chimera states in populations of nonlocally coupled chemical oscillators. *Phys. Rev. Lett.*, 110:244102, 2013. doi:10.1103/PhysRevLett.110.244102.
- [45] V. K. Jirsa, W. C. Stacey, P. P. Quilichini, A. I. Ivanov, and C. Bernard. On the nature of seizure dynamics. *Brain*, 137:2210, 2014. doi:10.1093/brain/awu133.
- [46] A. E. Motter, S. A. Myers, M. Anghel, and T. Nishikawa. Spontaneous synchrony in power-grid networks. *Nat. Phys.*, 9:191, 2013. doi:10.1038/nphys2535.
- [47] J. C. González-Avella, M. G. Cosenza, and M. San Miguel. Localized coherence in two interacting populations of social agents. *Physica A*, 399:24, 2014. ISSN 0378-4371. doi:https://doi.org/10.1016/j.physa.2013.12.035.
- [48] B. Hu, B. Li, and H. Zhao. Heat conduction in one-dimensional nonintegrable systems. *Phys. Rev. E*, 61:3828, 2000. doi:10.1103/PhysRevE.61.3828.
- [49] S. G. Matinyan and Y. Jack Ng. The partition function and level density for Yang–Mills–Higgs quantum mechanics. *J. Phys. A Math. Gen.*, 36:L417, 2003. doi:10.1088/0305-4470/36/25/102.
- [50] M. Zhan, Z. Zheng, G. Hu, and X. Peng. Nonlocal chaotic phase synchronization. *Phys. Rev. E*, 62:3552, 2000. doi:10.1103/PhysRevE.62.3552.
- [51] L. M. Pecora and T. L. Carroll. Synchronization in chaotic systems. *Phys. Rev. Lett.*, 64:821, 1990. doi:10.1103/PhysRevLett.64.821.
- [52] R. E. Amritkar and N. Gupte. Synchronization of chaotic orbits: The effect of a finite time step. *Phys. Rev. E*, 47:3889, 1993. doi:10.1103/PhysRevE.47.3889.
- [53] A. Ghosh and S. Chakraborty. Comprehending deterministic and stochastic occasional uncoupling synchronizations through each other. *Eur. Phys. J. B*, 93:113, 2020. doi:10.1140/epjb/e2020-100580-7.
- [54] R. Jeter and I. Belykh. Synchronization in on-off stochastic networks: Windows of opportunity. *IEEE Trans. Circuits Syst. I, Reg. Papers*, 62:1260, 2015. doi:http://ieeexplore.ieee.org/document/7097110/?reload=true.
- [55] L. Chen, C. Qiu, and H. B. Huang. Synchronization with on-off coupling: Role of time scales in network dynamics. *Phys. Rev. E*, 79:045101, 2009. doi:10.1103/PhysRevE.79.045101.
- [56] Y. Sun, Z. Ma, Liu F., and J. Wu. Theoretical analysis of synchronization in delayed complex dynamical networks with discontinuous coupling. *Nonlinear Dyn.*, 86:489, 2016. doi:10.1007/s11071-016-2902-2.
- [57] M. Schröder, S. Chakraborty, D. Witthaut, J. Nagler, and M. Timme. Interaction control to synchronize non-synchronizable networks. *Sci. Rep.*, 6:37142, 2016. doi:10.1038/srep37142(2016).
- [58] M. Cenk Eser, E. S. Medeiros, M. Riza, and A. Zakharova. Edges of inter-layer synchronization in multilayer networks with time-switching links. *Chaos*, 31:103119, 2021. doi:10.1063/5.0065310.
- [59] Z. Deng, S. Arsenault, C. Caranica, and et al. Synchronizing stochastic circadian oscillators in single cells of *Neurospora crassa*. *Nat. Commun.*, 6:35828, 2016. doi:https://doi.org/10.1038/srep35828.
- [60] F. Parastesh, H. Azarnoush, S. Jafari, B. Hatef, M. Perc, and R. Repnik. Synchronizability of two neurons with switching in the coupling. *Appl. Math. Comput.*, 350:217, 2019. ISSN 0096-3003. doi:https://doi.org/10.1016/j.amc.2019.01.011.
- [61] Z. Sun, N. Zhao, X. Yang, and W. Xu. Inducing amplitude death via discontinuous coupling. *Nonlinear Dyn.*, 92:1185, 2018. doi:10.1007/s11071-018-4117-1.
- [62] A. Ghosh, S. Mondal, and R. I. Sujith. Occasional coupling enhances amplitude death in delay-coupled oscillators. *Chaos*, 32:101106, 2022. doi:10.1063/5.0110203.

- [63] L. M. Pecora and T. L. Carroll. Master stability functions for synchronized coupled systems. *Phys. Rev. Lett.*, 80:2109, 1998. doi:10.1103/PhysRevLett.80.2109.
- [64] A. Ghosh, P. Godara, and S. Chakraborty. Understanding transient uncoupling induced synchronization through modified dynamic coupling. *Chaos*, 28:053112, 2018. doi:10.1063/1.5016148.
- [65] J. Tian, Y. Wang, and H. Qiu. Symmetry restoring dynamics in a two-species bosonic Josephson junction by using occasional coupling. *Commun. Theor. Phys.*, 72:055701, 2020. doi:10.1088/1572-9494/ab7ed0.
- [66] M. Albiez, R. Gati, J. Fölling, S. Hunsmann, M. Cristiani, and M. K. Oberthaler. Direct observation of tunneling and nonlinear self-trapping in a single Bosonic Josephson junction. *Phys. Rev. Lett.*, 95:010402, 2005. doi:10.1103/PhysRevLett.95.010402.
- [67] A. J. Leggett. Bose-Einstein condensation in the alkali gases: Some fundamental concepts. *Rev. Mod. Phys.*, 73:307, 2001. doi:10.1103/RevModPhys.73.307.
- [68] S. Raghavan, A. Smerzi, S. Fantoni, and S. R. Shenoy. Coherent oscillations between two weakly coupled Bose-Einstein condensates: Josephson effects, π oscillations, and macroscopic quantum self-trapping. *Phys. Rev. A*, 59:620, 1999. doi:10.1103/PhysRevA.59.620.
- [69] L. Fu and J. Liu. Quantum entanglement manifestation of transition to nonlinear self-trapping for Bose-Einstein condensates in a symmetric double well. *Phys. Rev. A*, 74:063614, 2006. doi:10.1103/PhysRevA.74.063614.
- [70] B. Juliá-Díaz, D. Dagnino, M. Lewenstein, J. Martorell, and A. Polls. Macroscopic self-trapping in Bose-Einstein condensates: Analysis of a dynamical quantum phase transition. *Phys. Rev. A*, 81:023615, 2010. doi:10.1103/PhysRevA.81.023615.
- [71] L. Zhang, X. Xu, and W. Zhang. The classical and quantum synchronization between two scattering modes in Bose-Einstein condensates. *Eur. Phys. J. Plus*, 135:202, 2020. doi:10.1140/epjp/s13360-020-00179-0.
- [72] H. Qiu, Y. Dong, H. Zhang, and J. Tian. Measure synchronization in hybrid quantum-classical systems. *Chinese Phys. B*, 31:120503, 2022. doi:10.1088/1674-1056/ac685c.
- [73] A. Ghosh, S. A. Pawar, and R. I. Sujith. Anticipating synchrony in dynamical systems using information theory. *Chaos*, 32:031103, 2022. doi:10.1063/5.0079255.
- [74] A. Ghosh. Early detection of synchrony in coupled oscillator model. *Eur. Phys. J. Plus*, 137:897, 2022. doi:10.1140/epjp/s13360-022-03122-7.
- [75] H. Zhang, H. Fan, Y. Du, L. Wang, and X. Wang. Anticipating measure synchronization in coupled Hamiltonian systems with machine learning. *Chaos*, 32:083136, 2022. doi:10.1063/5.0093663.
- [76] A. Barabási and M. Pósfai. *Network Science*. Cambridge University Press, first edition, 2016. ISBN 9781107076266.
- [77] G. Bianconi. *Multilayer Networks: Structure and Function*. OUP Oxford, first edition, 2018. ISBN 9780191068508.